ENERGETICS OF CLIMATE MODELS: NET ENERGY BALANCE AND MERIDIONAL ENTHALPY TRANSPORT

V. Lucarini[1,2,3] and F. Ragone[4]

[1] We analyze the publicly released outputs of the simulations performed by climate models (CMs) in preindustrial (PI) and Special Report on Emissions Scenarios A1B (SRESA1B) conditions. In the PI simulations, most CMs feature biases of the order of 1 W m^{-2} for the net global and the net atmospheric, oceanic, and land energy balances. This does not result from transient effects but depends on the imperfect closure of the energy cycle in the fluid components and on inconsistencies over land. Thus, the planetary emission temperature is underestimated, which may explain the CMs' cold bias. In the PI scenario, CMs agree on the meridional atmospheric enthalpy transport's peak location (around 40°N/S), while discrepancies of ~20% exist on the intensity. Disagreements on the oceanic transport peaks' location and intensity amount to ~10° and ~50%, respectively. In the SRESA1B runs, the atmospheric transport's peak shifts poleward, and its intensity increases up to ~10% in both hemispheres. In most CMs, the Northern Hemispheric oceanic transport decreases, and the peaks shift equatorward in both hemispheres. The Bjerknes compensation mechanism is active both on climatological and interannual time scales. The total meridional transport peaks around 35° in both hemispheres and scenarios, whereas disagreements on the intensity reach ~20%. With increased CO_2 concentration, the total transport increases up to ~10%, thus contributing to polar amplification of global warming. Advances are needed for achieving a self-consistent representation of climate as a nonequilibrium thermodynamical system. This is crucial for improving the CMs' skill in representing past and future climate changes.

1. INTRODUCTION

[2] The provision of an overarching picture of the climate system (CS) requires a detailed investigation of its global structural properties. Such an endeavor is of fundamental importance for understanding climate variability and climate change on a large variety of scales, which encompass major paleoclimatic shifts and almost regularly repeated events such as ice ages, as well as the ongoing and future anthropogenic climate change, as envisioned by the scientific program proposed in the landmark book by *Saltzmann* [2002].

[3] This effort has significant relevance also in the context of the ever increasing attention paid by the scientific community to the quest for reliable metrics to be used for the validation of climate models (CMs) of various degrees of complexity, as explicitly requested by the Fourth Assessment Report of the Intergovernmental Panel on Climate Change (IPCC4AR) [*Solomon et al.*, 2007], and for the definition of strategies aimed at the radical improvement of their performances, beyond incremental advances often obtained at the price of large increases in requested computing power. See the discussions by, e.g., *Lucarini* [2002], *Held* [2005], *Lucarini et al.* [2007, 2008], and *Lucarini* [2008]. European projects such as PRUDENCE, ENSEMBLES, and DEMETER; American initiatives such as the Third Coupled Model Intercomparison Project (CMIP3) developed within the Program for Climate Model Diagnosis and Intercomparison (PCMDI); and innovative volunteering activities as those organized by the British project climateprediction.net have greatly encouraged CMs' auditing. The pursuit of a "quantum leap" in climate modeling, which definitely requires new scientific ideas rather than just faster supercomputers, is becoming a key issue in the climate community [*Shukla et al.*, 2009].

[1]Department of Meteorology, University of Reading, Reading, UK.
[2]Department of Mathematics, University of Reading, Reading, UK.
[3]Walker Institute for Climate System Research, University of Reading, Reading, UK.
[4]Meteorologisches Institut, KlimaCampus, University of Hamburg, Hamburg, Germany.

[4] From a modern standpoint, the climate can be seen as a complex, nonequilibrium system, which generates entropy by irreversible processes; transforms moist static energy into mechanical energy [*Lorenz*, 1955, 1967] as if it were a heat engine [*Johnson*, 2000]; and, when the external and internal parameters have fixed values, achieves a steady state by balancing the input and output of energy and entropy with the surrounding environment [*Stone*, 1978b; *Peixoto and Oort*, 1992; *Ozawa et al.*, 2003]. The tools of phenomenological nonequilibrium thermodynamics [*Prigogine*, 1961; *de Groot and Mazur*, 1962] seem very well suited for defining a new point of view for the analysis of the CS [*Kleidon and Lorenz*, 2005; *Lucarini*, 2009a] and for understanding its variability and its large-scale processes, including the atmosphere-ocean coupling and the hydrological cycle. Moreover, such an approach seems valuable for understanding the mechanisms involved in climate phase transitions observed at the so-called tipping points, i.e., conditions under which catastrophes may occur for small variations in the boundary conditions or in the internal parameters of the system [*Lenton et al.*, 2008]. Recent results suggest that great progress in this direction is definitely within reach [*Lucarini et al.*, 2010a, 2010b].

[5] The energy driving the CS comes from the Sun in the form of shortwave radiation. Part of the radiation is scattered elastically back to space, with an efficiency which depends critically on the surface irradiated by the incoming light. Clouds and ice- and snow-covered and barren surfaces have, in general, the ability to scatter back to space relevant portions of the incoming radiation, while the process is much less efficient for, e.g., forested lands and especially the ocean surface. Albedo is commonly referred to as the fraction of the scattered with respect to the incoming radiation and is, in general, a two-dimensional time-dependent variable. The rest of the incoming radiation is absorbed by the fluid and solid components of the CS. The absorption process is not homogeneous in space and time because of variability in the amount of incoming energy and because the interaction of radiation with matter depends critically on the nature and density of the irradiated medium. Most of the net incoming solar radiation is absorbed at the surface and is redistributed throughout the atmospheric column by a variety of means such as convection, latent and sensible heat fluxes, and longwave radiative exchanges within the atmosphere and between the atmosphere and the underlying surface. Organized and turbulent atmospheric motions and the hydrological cycle (including the formation and dissipation of clouds) are the direct result of this process of energy redistribution. Oceanic motions are also generated, basically as an outcome of the variable exchange of heat, water, and momentum between the water masses and the overlying atmosphere.

[6] Energy is irradiated back to space in the form of longwave radiation approximately thermalized at temperatures typical of the CS, so that on the global average the net incoming solar radiation is approximately compensated by the outgoing longwave radiation. Since clouds have a great impact in determining both the amount of scattered solar

radiation (because of their typically high albedo) and the amount of outgoing longwave radiation (because of their typically high emissivity), they have a crucial role in modulating the local and global net energy balance. On a planetary scale, large-scale atmospheric and oceanic motions allow for the reduction of the temperature difference between high and low latitudes in both hemispheres with respect to what would be enforced by purely local radiative and convective processes. The low- and high-latitude regions differ largely in terms of net incoming radiation, because of astronomical factors and local albedo properties, and feature opposite signs of the net balance of the radiative flux at the top of the atmosphere (TOA). In general, we understand that the so-called differential heating, both in the small and in the large scales, is the basic ingredient of the nonequilibrium nature of the CS [*Lorenz*, 1967; *Peixoto and Oort*, 1992]. The described processes have relevant impacts also in terms of the second law of thermodynamics as in the CS, entropy production is inextricably related to the irreversible heat transfer from high- to low-temperature regions [*Goody*, 2000; *Ozawa et al.*, 2003; *Lucarini et al.*, 2010a, 2010b].

[7] Therefore, it seems of the greatest importance to devote attention to the analysis of the consistency of the state-of-the-art CMs in the representation of the net energy balance and entropy production and transport in the CS as a whole as well as in its main subdomains. While the analysis of entropy production will be the subject of a separate publication, along the lines of *Ozawa et al.* [2003] and *Wu and Liu* [2010], we hereby wish to focus on the analysis of energetics of the CS in selected simulations of the CMs included in the IPCC4AR, by taking advantage of the immense data repository provided by the PCMDI CMIP3 project.

[8] In this work we analyze the behavior of the CMs under steady state conditions, thus taking advantage of the data produced with the preindustrial scenario, where CMs are integrated for several hundreds of years with fixed atmospheric composition with 280 ppm CO_2 concentration. We also aim to understand how different the CMs' responses are to the CO_2 radiative forcing impacts. For this latter purpose, we have considered the CMs' outputs produced under the Special Report on Emission Scenario A1B (SRESA1B) scenario, which foresees a stable CO_2 concentration of 720 ppm after 2100 following a prolonged increase after 2000. The initial conditions of the SRESA1B runs are provided by the final state of the 20th century runs, which are, in turn, initialized in the second half of the 19th century using the outputs of the preindustrial runs as initial conditions. Since we wish to avoid the period of direct forcing and focus on the time frame when CMs start to relax toward the steady state, we analyze data referring to the 22nd and 23rd centuries.

1.1. Net Global Balances in a Steady State

[9] Following and expanding previous analyses [*Wild et al.*, 2006; *Wild*, 2008; *Trenberth et al.*, 2009; *Trenberth and Fasullo*, 2009, 2010b], we first perform a thorough audit of the CMs in their representation of the net energy balance of the whole CS and, separately, of the atmo-
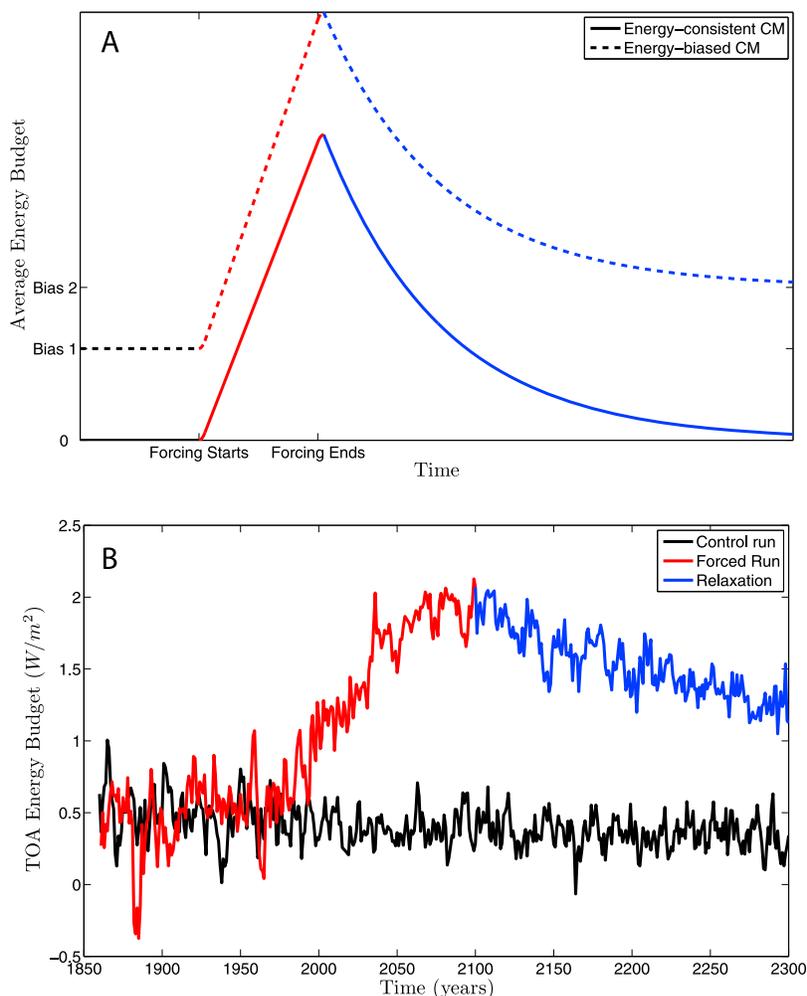
Figure 1. (a) Idealized time dependence of the TOA global energy budget as given by a CM which has a self-consistent representation of energy exchange processes (solid line) versus an energy biased CM. Black, red, and blue lines show the initially unperturbed runs, the forced runs, and the runs performed with newly established fixed parameters, respectively. (b) Smoothed (5 year filter) yearly time series of the GFDL2.1 model (CM 9) TOA energy budget. The black line shows the preindustrial run. The red-line shows the 20th century simulation (started from year 1 of the preindustrial run) and the 21st century portion of the SRESA1B simulations (started from the end of the 20th century simulation). The blue line shows the 22nd and 23rd century SRESA1B simulation.

sphere, of the ocean, and of the land, in order to test how consistently steady state conditions are realized in the case of preindustrial simulations. Moreover, by comparing the obtained results with the net energy balances obtained from the runs performed under SRESA1B conditions, we understand how the CMs describe the CS response to time-dependent CO_2 radiative forcing.

[10] As discussed above, basic physical principles suggest that under generic boundary conditions the ultimately realized steady state obeys general zero-sum properties for energy fluxes [*Prigogine*, 1961; *Peixoto and Oort*, 1992]. Therefore, when statistical stationarity is eventually obtained after transients have died out, a physically consistent (even if not necessarily realistic in the representation of each and every climatic feature) CM should feature a vanishing (when long time averages are considered) net energy bal-

ance as a whole and for any of its subdomains. If this is not the case, the energy bias of the CM has to be attributed to unphysical energy sources or sinks. We remark that this property has nothing to do with the so-called operation of "model tuning": a CM with a bad parametric tuning probably features inaccurate or even unrealistic climate properties, but if the CM is energetically consistent and steady state is attained, the net energy balance for any subdomain should be vanishing, on average.

[11] Figure 1a contrasts the idealized behavior of a CM whose energy exchange processes are consistent (solid line) with that of a biased CM (dashed line). In the former case, in the initial steady state conditions (black line) the net TOA average energy balance vanishes, whereas in the latter a spurious bias (bias 1 in Figure 1) is present. When the parameters of the system are changed with time so that

forcing is applied (red line), both models foresee a non-vanishing net TOA balance (positive in this representation, as in global warming conditions). When the parameters are held fixed to newly established values, the system relaxes toward the new steady state within a time comparable to a few units of the slowest of the internal time scales (the oceanic one, in usual climate conditions). While the energy-consistent model readjusts toward a zero TOA energy balance, the other model's net TOA energy balance will readjust toward a nonvanishing bias, generically different (and so climate dependent) from the initial one. Note that whereas in the case of a good model the net total heating resulting from the forcing corresponds to the integral of the net energy balance, in the case of an imperfect model with potentially climate-dependent bias the net heating of the system is, in principle, ill defined. Conceptually analogous cartoons actually apply not only to the net global energy balance but also to the net energy balance of any climatic subdomains, with the crucial difference that the slowest internal time scale will be faster for, e.g., the atmosphere than for the ocean.

[12] Given the complexity of the processes inside the climate system and the fact that large cancelations are involved when computing the budget, the provision of a consistent or at least reasonable net energy balance is, in general, far from being an obvious task, so that an extensive CMs intercomparison analysis is necessary to understand to what extent the actual CMs will conform to the case depicted in Figure 1a.

[13] In the case of reanalyses, the bias in the diagnosed net global energy balance is of the order of -10 W m^{-2}, which is about 1 order of magnitude larger in absolute value (and wrong in the sign) than the reasonably expected imbalance due to the anthropogenic and natural forcings in the second half of the 20th century. Surprisingly, the performance of these data sets for this specific benchmark does not improve even after 1979, which marks the beginning of the massive assimilation of satellite data [*Yang et al.*, 1999; *Allan et al.*, 2004].

[14] Moreover, in spite of ever increasing and improving sources of observational data from satellites on incoming and outgoing radiation at the TOA, it is very hard to restrict the uncertainties on the observed yearly averaged energy balance of the planet to the order of 1 W m^{-2} [*Kiehl and Trenberth*, 1997; *Trenberth et al.*, 2009]. Very recently, it has been emphasized how important it is to correctly track the Earth's energy budget in models and observations for understanding climate change and variability [*Trenberth and Fasullo*, 2010b].

[15] Additional motivations for checking the net energy balance of CMs emerge from potential drawbacks in the numerical representation of the dynamics of fluid media. Some studies have shown that numerical codes commonly adopted for the representation of the dynamics of geophysical fluids are not necessarily energy conserving, as kinetic energy losses due to friction and diffusion are not exactly fed back in the system as thermal forcing, and that commonly adopted hyperdiffusive schemes seem to be especially problematic in this regard [*Becker*, 2003; *Lucarini and Fraedrich*, 2009].

1.2. Transports

[16] When considering global energy balances the CS is reduced to a zero-dimensional system. We then take a step forward and tackle the problem of models' representation of the meridional enthalpy transport by the CS as a whole and by the atmosphere and the ocean separately. In order to achieve steady state, a net positive TOA energy balance in a given location must be compensated, when long-term averages are considered, by a net divergence of the enthalpy flux.

[17] The net TOA energy balance of the planet has to a very good approximation a zonal structure, with low-latitude regions featuring a positive imbalance between the net input of solar radiation (controlled by incoming solar radiation and albedo) and the output of longwave radiation (controlled by surface temperature, water vapor concentration, and clouds). A negative imbalance is instead observed in high-latitude regions [*Peixoto and Oort*, 1992]. Therefore, on average, the fluid envelope of the CS transports large amounts of heat from low- to high-latitude regions in both hemispheres [*Stone*, 1978a; *Schneider*, 2006]. See *Frierson et al.* [2007] and *Vallis and Farneti* [2009] for recent theoretical treatments in a rather general setting.

[18] It is then found that in each hemisphere the maximum intensity of the meridional transport is in the long term equal to the absolute value of the total positive energy imbalance in the low-latitude region (or, equivalently, the energy deficit in the high-latitude region), whereas its maximum is located at the "transition" latitude where the TOA energy balance vanishes [*Peixoto and Oort*, 1992; *Schneider*, 2006]. Therefore, the location and the intensity of the maximum of the transport provide fundamental information on the properties of the CS. On the other hand, large-scale organized atmospheric and oceanic motions result from the mechanical work (then dissipated in a turbulent cascade) produced by the climate engine through the Lorenz energy cycle, which is fueled essentially by the presence of temperature differences across the CS [*Lorenz*, 1967]. Recently, a rather complete picture of the Lorenz energy cycle in simple yet rigorous thermodynamic terms has been provided [*Johnson*, 2000] and linked to estimates of the turbulent entropy production of the planet [*Lucarini*, 2009a].

[19] Earlier reconstructions of the meridional transport using interpolations of radiosonde data (with unavoidable uncertainties due to the uneven spatial coverage and homogeneity issues of the data sets) suggested a comparable contribution to the meridional transport by the ocean and by the atmosphere [*Peixoto and Oort*, 1992]. Instead, more recent data suggest that especially in the Southern Hemisphere, the atmospheric transport definitely plays a dominant role [*Trenberth and Caron*, 2001].

[20] Many properties of the CS play an important role in determining the properties of the meridional atmospheric and oceanic transport, the main being the meridional gradient

of the planetary albedo. Moreover, on Earth the mechanisms of transport are rather different in the Northern and Southern Hemisphere. In the Northern Hemisphere, considerable contributions to the meridional transport are given, separately, by the transient and stationary waves of the atmosphere as well as by the ocean. Instead, in the Southern Hemisphere, most of the transport is performed by transient atmospheric waves only. Nonetheless, the maximum value and the location of the peak of the transport are very similar in the two hemispheres [*Trenberth and Caron*, 2001].

[21] Indeed, some basic features of the transport profile seem to be symmetric with respect to the equator as they are constrained by basic fluid dynamical laws and by the geometrical properties of the system. In a classic paper, *Stone* [1978b] showed that in a planet the climatological total meridional transport profile (and especially the position of its peak) is determined, to the first order of approximation, by spherical geometry and latitudinal dependence of TOA incoming radiation only. See also *Enderton and Marshall* [2009] for a recent reexamination of this brilliant idea.

[22] Since we still do not have a comprehensive rigorous theory that is able to express the peak location and strength of the meridional transport and to accommodate the variety of processes contributing to it, it seems crucial to test the degree of realism and consistency of CMs in representing these basic climatic features. The direct calculation of the transports from 3-D climate fields requires very serious diagnostic tools and high-resolution data (in time) since quadratic quantities are involved. Nevertheless, under the assumption of steady state conditions and of no biases in the energy balances of the whole CS, of the atmosphere, and of the ocean, it is possible to rigorously reconstruct the meridional enthalpy transport by atmosphere and ocean from the zonal averages of the heat fluxes at the upper and lower boundaries of the fluid envelope [*Peixoto and Oort*, 1992]. Even in the presence of biases in the net energy balances (if these are small enough with respect to the latitudinal variability) such a reconstruction technique can be safely adopted with minor corrections, as discussed by *Carissimo et al.* [1985] and by *Trenberth and Caron* [2001]. The meridional transport profiles provide a very strong characterization of the CMs, and it seems pivotal to intercompare their performances in order to understand how well they agree in the representation of such relevant climatic properties. Moreover, the analysis of the response to CO_2 increase of the meridional transport probably provides the most basic way of investigating the adjustment of the dynamics of the fluid components of the CS.

1.3. Goals and Structure of the Paper

[23] The overall goal of this paper is to present a complete review of the state of the art of climate modeling in terms of its representation of the CS energetics and of the energetics of ocean and atmosphere separately. The authors also wish to stimulate lines of activities aimed at improving the reliability of CMs, which is a task of the uttermost urgency in the context of preparation of future IPCC reports. The paper

is organized as follows: In section 2, starting from the Eulerian energy balance equations, we briefly recapitulate the equations determining the energy budget of the CS and of its subdomains and show how the meridional transport can be inferred. In section 3 we present the data considered in this work and discuss the methods used in their processing. In section 4 we present our results, in section 5 we discuss our findings, and in section 6 we give our conclusions and provide perspectives for future work.

2. ENERGY BUDGET IN THE CLIMATE SYSTEM

[24] In this section we review the derivation of the zonally and globally integrated energy budget of the CS and of its subdomains and show how, assuming steady state conditions, it is possible to infer the meridional enthalpy transport by the atmosphere, by the ocean, and by the system as a whole. We also discuss how to estimate the transport profiles when energy budgets are not perfectly closed because of actual deviations from steady state or spurious biases in the data.

2.1. Instantaneous Balance Equations

[25] The evolution equation in Eulerian form for the total energy density e in the fluid component of the Earth system, given by the sum of the kinetic and moist static potential components, can be written as [*Peixoto and Oort*, 1992]

$$\frac{\partial \rho e}{\partial t} = -\nabla \cdot (\rho e \mathbf{c}) - \nabla \cdot \mathbf{F_R} - \nabla \cdot \mathbf{F_S} - \nabla \cdot \mathbf{F_L} - \nabla \cdot (p\mathbf{c} + \tau \cdot \mathbf{c}),$$

(1)

where ρ is the density; t is time; $\mathbf{c}$ is the velocity vector; $\mathbf{F_R}$, $\mathbf{F_S}$, and $\mathbf{F_L}$ are the vectors of the radiative, turbulent sensible, and turbulent latent heat fluxes, respectively; p is the pressure; and τ is the stress tensor. It is useful to rewrite equation (1) as

$$\frac{\partial \rho e}{\partial t} = -\nabla \cdot \mathbf{J_h} - \nabla \cdot \mathbf{F_R} - \nabla \cdot \mathbf{F_S} - \nabla \cdot \mathbf{F_L} - \nabla \cdot (\tau \cdot \mathbf{c}), \quad (2)$$

where we have introduced the total enthalpy transport $\mathbf{J_h} = (\rho e + p)\mathbf{c} = \rho h \mathbf{c}$, where the standard definition of enthalpy $h = e + p/\rho$ is adopted [*Fermi*, 1956; *Kundu and Cohen*, 2008]. Note that more commonly, the expression "energy" or "heat transport" is adopted in the literature [*Peixoto and Oort*, 1992]. As discussed by *Ambaum* [2010], equation (2) expresses a local balance corresponding to the first law of thermodynamics for an open system, and enthalpy (rather than energy or heat) transports enter the picture because exchange of mass takes place. Note also that since all terms on the right-hand side of equations (1) and (2) are written as convergence of vector fields, by using Gauss's theorem it is easy to obtain an expression for the derivative of the total energy content of a subdomain of the CS in terms of the fluxes at the boundary.

[26] Expressing the divergence operator in spherical coordinates and taking the usual thin shell approximation

so that $R + z \approx R$, where R is the radius of the planet and z is the vertical coordinate, we obtain

$$\frac{\partial \rho e}{\partial t} = -\frac{1}{R\cos\varphi}\frac{\partial J_{h\lambda}}{\partial \lambda} - \frac{1}{R\cos\varphi}\frac{\partial J_{h\varphi}\cos\varphi}{\partial \varphi} - \frac{\partial J_{hz}}{\partial z}$$
$$+ -\frac{\partial}{\partial z}\left[F_{Rz} + F_{Sz} + F_{Lz} + (\tau \cdot \mathbf{c})_z\right], \tag{3}$$

where λ is the longitude, φ is the latitude, and in the last term of equation (3) we have retained only the vertical components of the radiative and turbulent fluxes and of the contributions due to frictional stresses since they are largely dominant by various orders of magnitude [*Peixoto and Oort*, 1992] with respect to the horizonal components. In order to characterize the large-scale properties of the CS, we need to analyze the properties of the temporal and spatial averages of the net energy balance. It is particularly relevant to exploit equation (3) to study the interaction between the various climatic subsystems. Let Ω be a subdomain of the CS. For our purposes, Ω will refer to the atmosphere ($\Omega = A$), the ocean ($\Omega = O$), or the land subdomain ($\Omega = L$), as well as the complete system ($\Omega = T$). Given a generic field $a = a(t, \lambda, \varphi, z)$, we denote as "mass weighted vertical integral" of a over Ω the integral

$$A_\Omega(t, \lambda, \varphi) \equiv \int_{z_b}^{z_t} \rho\, a(t, \lambda, \varphi, z')\mathrm{d}z', \tag{4}$$

where z_b and z_t are the lower and the upper boundaries, respectively, that delimit Ω. Note that where the thickness of the subdomain Ω is vanishing (for example, $\Omega = O$ and the coordinates (λ, φ) correspond to continental areas), equation (4) is still well defined as $A_\Omega(t, \lambda, \varphi)$ results automatically in zero. We can then define the "zonal integral":

$$[A_\Omega](t, \varphi) \equiv \int_0^{2\pi} A_\Omega(t, \lambda', \varphi)R\cos\varphi\, \mathrm{d}\lambda'. \tag{5}$$

[27] In order to characterize the one-dimensional structure of the system, we zonally and vertically integrate equation (3). For the entire planet ($\Omega = T$) we have

$$[\dot{E}_T] = -\frac{1}{R}\frac{\partial T_T}{\partial \varphi} + [F_R]_{\text{TOA}}, \tag{6}$$

where $[\dot{E}_T]$ is net energy balance of the entire planet, $[F_R]_{\text{TOA}}$ is the zonal mean of F_R evaluated at TOA, and

$$T_T(t, \varphi) = \int_0^{2\pi}\int_{z_b}^{\text{TOA}} J_{h\varphi}(t, \lambda', \varphi, z')R\cos\varphi\, dz'd\lambda' \tag{7}$$

is the total transport of enthalpy realized through the latitudinal wall at latitude φ, with z_b being the bottom of the ocean.

Similarly, we can derive the equations for the atmosphere, ocean, and land:

$$[\dot{E}_A] = -\frac{1}{R}\frac{\partial T_A}{\partial \varphi} + [F_R]_{\text{TOA}} + [F_R + F_S + F_L]_{\text{surf},A}, \tag{8}$$

$$[\dot{E}_O] = -\frac{1}{R}\frac{\partial T_O}{\partial \varphi} - [F_R + F_S + F_L]_{\text{surf},O}, \tag{9}$$

$$[\dot{E}_L] = -[F_R + F_S + F_L]_{\text{surf},L}, \tag{10}$$

where the subscripts in the last terms on the right-hand sides of equations (8)–(10) refer to the boundary considered. Moreover,

$$T_A(\varphi) = \int_0^{2\pi}\int_{z_s}^{\text{TOA}} J_{h\varphi}(t, \lambda', \varphi, z')R\cos\varphi\, \mathrm{d}z'\mathrm{d}\lambda' \tag{11}$$

$$T_O(\varphi) = \int_0^{2\pi}\int_{z_b}^{z_s} J_{h\varphi}(t, \lambda', \varphi, z')R\cos\varphi\, \mathrm{d}z'\mathrm{d}\lambda' \tag{12}$$

are the atmospheric and oceanic total transports through the latitudinal wall at latitude φ, respectively, while z_s is the surface level. Since land is not a fluid subdomain of the system, the large-scale enthalpy transport through this medium is entirely negligible, so that no transport term is present in equation (10). We have neglected the transfer of mechanical energy from the atmosphere to the ocean since it is smaller by some orders of magnitude than the other energy exchange terms [*Peixoto and Oort*, 1992]. Such a term is instead of great importance when considering the driving mechanisms of the large-scale ocean circulation [*Kuhlbrodt et al.*, 2007]. Note that the fact that this term is so small compared to the thermal energy fluxes is related to the very low efficiency of the CS as a whole [*Lucarini*, 2009a].

[28] If we further integrate equations (6) and (8)–(10) over latitude from $-\pi/2$ to $\pi/2$, we obtain the following expressions for the time derivative of the net global energy balance and for the net energy balance of the atmosphere, the ocean, and the land:

$$\{\dot{E}_T\} = \{F_R\}_{\text{TOA}}, \tag{13}$$

$$\{\dot{E}_A\} = \{F_R\}_{\text{TOA}} + \{F_R\}_{\text{surf},A} + \{F_S\}_{\text{surf},A} + \{F_L\}_{\text{surf},A}, \tag{14}$$

$$\{\dot{E}_O\} = -\{F_R\}_{\text{surf},O} + \{F_S\}_{\text{surf},O} + \{F_L\}_{\text{surf},O}, \tag{15}$$

$$\{\dot{E}_L\} = -\{F_R\}_{\text{surf},L} + \{F_S\}_{\text{surf},L} + \{F_L\}_{\text{surf},L}, \tag{16}$$

where we have defined

$$\{X\}(t) = \int_{-\pi/2}^{\pi/2} [X](t, \varphi)R\, \mathrm{d}\varphi \tag{17}$$

for a generic variable $[X](t, \varphi)$.

2.2. Time Averages

[29] If the system is forced with the usual seasonal cycle and the internal and external parameters of the system are not time dependent, we expect that after a suitable transient, steady state conditions are realized. As different domains of the climatic system have different internal time scales, the realization of steady state conditions occurs in a large variety of time horizons when the system is initialized from arbitrary initial conditions or when parameters are suddenly altered. In general, when time-dependent forcings in the form of parametric variations are present, a climatic subsystem is in quasi-steady conditions when its internal time scales are much faster than the characteristic time scale of the parametric change. In this case, the subsystem is driven by the parametric modulation of the forcing. The atmosphere and land subdomains have a much shorter time scale than the ocean. The atmosphere and the land can be considered to be balanced over time scales of less than 1 year, while the ocean features time scales ranging from some years to several hundreds of years. The current climate radiative forcing (and, arguably, those projected under the SRESA1B scenario) is slow enough that the atmosphere can be expected to be in quasi steady state conditions, whereas the ocean lags behind [Solomon et al., 2007]. Following Saltzmann [2002], we can define the atmosphere and land subdomains as "thin" climatic subdomains, while the ocean is a "thick" subdomain. The presence of interacting subsystems with very different characteristic time scales is one of the key elements of complexity of the CS.

[30] Under steady state conditions, the long-term average of the derivative of any climatic fields needs to vanish because otherwise, trends would be present. When long-term averages are applied to equations (13)–(16), we obtain the general formula

$$\overline{\{\dot{E}_\Omega\}} = \overline{\{B_\Omega\}} = 0, \tag{18}$$

where the overbar indicates the time averaging operation and B_Ω is the algebraic sum of the fluxes entering the domain thorough the upper and lower boundaries of the domain Ω. Instead, the time average of the zonally and vertically integrated energy equation for a generic domain Ω can be written as

$$\overline{[\dot{E}_\Omega](\varphi)} = -\frac{1}{R}\frac{\partial \overline{T_\Omega}}{\partial \varphi} + \overline{[B_\Omega]}. \tag{19}$$

Under steady state conditions, the left-hand side of equation (19) vanishes, so that the average transport $\overline{T_\Omega}$ can be computed as

$$\overline{T_\Omega}(\varphi) = -\int_\varphi^{\pi/2} \overline{[B_\Omega]}(\varphi')R\, \mathrm{d}\varphi'. \tag{20}$$

[31] Since basically no substantial large-scale enthalpy transport can take place through a solid medium, in stationary conditions the surface energy fluxes over land are expected to be locally vanishing when long-term averages are considered. Instead, nonvanishing sustained local energy imbalances are possible at the atmospheric and oceanic interface and at TOA since they are compensated by the divergence of the enthalpy transport realized by the motions of the system.

[32] Geometry imposes that we should have zero meridional transport at the poles. In agreement with that, equation (20) imposes $\overline{T_\Omega} = 0$ at $\varphi = \pi/2$ (North Pole). Moreover, in steady state conditions the net energy balance $\overline{\{B_\Omega\}}$ is expected to vanish, so that consistently, $\overline{T_\Omega}$ is zero also at $\varphi = -\pi/2$ (South Pole).

[33] As suggested by Carissimo et al. [1985] and by Trenberth and Caron [2001], the procedure of inferring meridional transports from zonal energy balances can be considered robust enough also in the case of non-steady state conditions and inhomogeneous information, as when gathering from various sources observational estimates on the energy balance in present climate conditions. The condition for the applicability of this procedure is that the latitudinal variability of $\overline{[B_\Omega]}(\varphi)$ should be much larger than $\overline{\{B_\Omega\}}/(2\pi R)$, which is easily met in terrestrial conditions for the outputs of climate simulations (see section 4). Nevertheless, in order to have vanishing transport also at $\varphi = -\pi/2$ we need to correct equation (20). The simplest way to accomplish that [Carissimo et al., 1985] is to redefine $\overline{T_\Omega}$ as follows:

$$\overline{T_\Omega}(\varphi) = -\int_\varphi^{\pi/2} \overline{[B_\Omega]}^{\mathrm{corr}}(\varphi')R\, \mathrm{d}\varphi', \tag{21}$$

where

$$\overline{[B_\Omega]}^{\mathrm{corr}}(\varphi) = \overline{[B_\Omega]}(\varphi) - \overline{\{B_\Omega\}}/2\pi R. \tag{22}$$

This amounts to assuming a constant flux correction throughout the surface. Different approaches, based on, e.g., differently weighting various latitudinal belts on the basis of the a priori knowledge of the data uncertainties, provide rather similar outputs when biases are overall small as in our case. Therefore, throughout this paper we will stick to the definition given in equation (21).

3. DATA AND METHODS

3.1. Data Set

[34] The PCMDI CMIP3 (http://www-pcmdi.llnl.gov/) is a CM intercomparison project run by the Lawrence Livermore National Laboratories (USA) freely providing access to a vast data set of outputs of standardized simulations performed by state-of-the-art CMs under various past, present, and future climate scenarios. The PCMDI CMIP3 includes data from over 20 CMs and has been a key contribution to the IPCC4AR since it has provided a large community of scientists with the possibility of extensively and systematically analyzing the performances of many CMs on the same test beds and has greatly stimulated the development of metrics to be used for intercomparison and validation studies. Presently, the new initiative PCMDI CMIP5 (http://cmip-pcmdi.llnl.

TABLE 1. Models Considered in This Work, Institutions, and Data Availability in Each Considered Time Period[a]

Model Number	Model	Institution	PI	SRESA1B 2101–2200	SRESA1B 2201–2300
1	BCCR-BCM2.0	Bjerknes Center, Norway	yes	no data	no data
2	CGCM3.1 (T47)	CCCma, Canada	flux adjustment	flux adjustment	flux adjustment
3	CGCM3.1 (T63)	CCCma, Canada	flux adjustment	flux adjustment	flux adjustment
4	CNRM-CM3	Météo France, France	yes	yes	2101–2299
5	CSIRO-Mk3.0	CSIRO, Australia	80 years, no surface	no data	no data
6	CSIRO-Mk3.5	CSIRO, Australia	yes	no data	no data
7	FGOALS-g1.0	LASG, China	yes	yes	no data
8	GFDL-CM2.0	GFDL, USA	yes	yes	yes
9	GFDL-CM2.1	GFDL, USA	yes	yes	yes
10	GISS-AOM	NASA GISS, USA	yes	no data	no data
11	GISS-EH	NASA GISS, USA	no surface	no data	no data
12	GISS-ER	NASA GISS, USA	no surface	no surface	2201–2297, no surface
13	HADCM3	Hadley Centre, UK	yes	2108–2199	no data
14	HADGEM	Hadley Centre, UK	99 years	2101–2199	no data
15	INM-CM3.0	Institute of Numerical Mathematics, Russia	yes	yes	no data
16	IPSL-CM4	IPSL, France	yes	yes	2201–2231
17	MIROC3.2 (hires)	CCSR, NIES, and FRCGC, Japan	yes	no data	no data
18	MIROC3.2 (medres)	CCSR, NIES, and FRCGC, Japan	yes	yes	yes
19	ECHO-G	MIUB and Max-Planck-Institut (Germany) and METRI (Korea)	flux adjustment	flux adjustment	flux adjustment
20	ECHAM5/MPI-OM	Max-Planck-Institut, Germany	yes	no surface	no surface
21	MRI-CGCM2	Meteorological Research Institute, Japan	flux adjustment	flux adjustment	flux adjustment
22	NCAR CCSM	NCAR, USA	no data	no data	no data
23	NCAR PCM	NCAR, USA	no data	2101–2199, no surface	no data

[a]Each model is labeled with a number. Exclusion of TOA data for CM 22 (available from the PCMDI CMIP3 data set) is based upon the discussion given by *Trenberth and Fasullo* [2010a]. PI, preindustrial; CCCma, Canadian Centre for Climate Modelling and Analysis; CSIRO, Commonwealth Scientific and Industrial Research Organisation; LASG, National Key Laboratory of Numerical Modeling for Atmospheric Sciences and Geophysical Fluid Dynamics; GFDL, Geophysical Fluid Dynamics Laboratory; NASA GISS, NASA Goddard Institute for Space Studies; IPSL, Institut Pierre-Simon Laplace; CCSR, Center for Climate System Research; NIES, National Institute for Environmental Studies; FRCGC, Frontier Research Center for Global Change; MIUB, Meteorologischen Institut der Universität Bonn; METRI, National Institute of Meteorological Research; NCAR, National Center for Atmospheric Research.

gov/cmip5/) is being set up along similar lines to support the preparation of the Fifth IPCC Assessment Report. Data referring to this new generation of climate simulations should become available in the second half of 2011.

[35] In this paper, we are interested in analyzing the behavior of the CMs in two standard IPCC4AR scenarios: (1) the preindustrial scenario, where the CS is integrated with fixed parameters and, in particular, with fixed CO_2 concentration set at 280 ppm until steady state conditions with no apparent trend in the climatic variables are observed, and (2) the SRESA1B scenario, characterized by a constant increase of CO_2 from 2000 to 2100, when 720 ppm concentration is obtained and subsequently kept constant. It would have been interesting also to compare two different steady states (e.g., preindustrial versus $2\times CO_2$ conditions) in order to characterize the generalized climate sensitivities of the system, but unfortunately, the $2\times CO_2$ control run data provided in the PCMDI CMIP3 data sets refer to slab ocean integrations and therefore are of limited use.

[36] In spite of the overall purpose of PCMDI CMIP3 of providing complete and standardized data sets, we have found some deficiencies in data availability, which lead to difficulties in performing a complete and systematic intercomparison analysis. This calls for further improvements for initiatives following the magnificent efforts by PCMDI CMIP3. A typical problem has been the lack of one or more surface fields for a CM in a certain scenario, which has

restricted the analysis to TOA properties only. In some cases, TOA fields are also lacking, so that the corresponding CM is simply excluded from the analysis for that scenario. Moreover, some CMs have corrupted data for certain fields or incorrect metadata accompanying the data sets. Therefore, some data have been directly obtained from the modeling centers.

[37] Other inconsistencies are related to the temporal window of the data provided for different CMs for a given scenario. Regarding the preindustrial scenario, the various CMs present time series of data of different lengths. In our case, we have chosen 100 years as the standard length of the time series to be analyzed. However, some CMs present less than 100 years of data. We have decided to perform the analysis also on these CMs, operating on the available data. Regarding the SRESA1B scenario, not all the CMs present data for the 22nd *and* for the 23rd centuries: some CMs' data stop at 2200, and others even stop at 2100 (before stabilization of CO_2 has begun). Again, we have operated on all the available data after 2100. Finally, we have made the radical choice of excluding the models with flux adjustments since their energetics are intrinsically biased. First, an unphysical energy flux is added between the atmosphere and the ocean, so that the consistency of their separate net energy balances is adversely affected. Second, a more serious inconsistency is realized when flux adjustment is applied over land surface since a spurious

source/sink of energy is added to the fluid component of the climate system. An exception has been made for the INM-CM3.0 model since the flux adjustments are present only in a very limited oceanic region, so that no substantial impacts are expected at the global level and for zonally integrated quantities. An overview of the CMs considered in this study and of the data availability of the scenario runs is given in Table 1. Each CM is labeled by an identifying number: this convention is used throughout the text and in Figures 2–5 and 7–12.

[38] In the optimal scenario, we have considered for both climate scenarios the fields of shortwave and longwave radiation fluxes at TOA and at the surface, plus the fields of latent and sensible heat fluxes at the surface. Radiative fluxes as well as latent and sensible heat fluxes are expressed in W m^{-2}. Moreover, we have taken into account the land-sea mask, which quantifies the portion of surface covered by sea and by land. Depending on the considered CM, the values of the land-sea mask can be either Boolean (0 = sea and 1 = land) or continuous between 0 and 1, thus allowing for mixed coverage. Fields relative to the energy fluxes are 2+1 dimensional, being time series of bidimensional fields, while the land-sea mask is a fixed bidimensional field. Since we are interested in yearly averages, we have reduced the computational and storage burden of our facilities by downloading only preprocessed monthly mean fields and then using them to compute the annual means. Data have been downloaded in netcdf format, have then been imported in the MATLAB 7.0$^{®}$ environment with the freely available Commonwealth Scientific and Industrial Research Organisation netCDF/ OPeNDAP software (http://www.marine.csiro.au/sw/matlab-netcdf.html), and have eventually been processed with in-house scripts.

[39] Note that in agreement with the actual estimates for the present climate [*Peixoto and Oort*, 1992], the surface average of the transfer of mechanical energy from the atmosphere in the ocean is in all models and in both scenarios positive and of the order of 10^{-2} W m^{-2} at most. This term is several orders of magnitude smaller than the absolute value of the other terms contributing to the atmospheric and oceanic energy budgets and also much smaller than the net values of the net energy budgets we will discuss in section 4. Therefore, we can safely neglect this contribution.

3.2. Statistical Estimators

[40] In the preindustrial control runs, since the slowest external forcing to the system is the seasonal cycle (no variability of the incoming solar radiation is considered), steady state conditions are expected to hold. Therefore, the time series of the yearly zonally integrated $\langle[B_\Omega]\rangle_j$ and globally integrated energy balance $\langle\{B_\Omega\}\rangle_j$ (where j refers to the jth of the N years) are expected to have vanishing expectation values for each domain Ω. Thus, for a given Ω, the yearly meridional transport one-dimensional fields $\langle T_\Omega(\varphi)\rangle_j$ computed by applying equation (21) are expected to be statistically equivalent.

[41] For the 22nd and 23rd century SRESA1B scenario outputs, the slowest forcing is also the seasonal cycle, so that generating the time series of yearly averaged values is a sensible operation. Nevertheless, as the system is readjusting to a new steady state, we may expect to see trends in the yearly data related to slow subsystems, i.e., the whole CS and the ocean subdomain. Actually, we find an approximate exponential behavior with decaying time which can be estimated as being of the order of 500–700 years, which nicely matches the characteristic time scale of the large-scale ocean circulation [*Kuhlbrodt et al.*, 2007]. For the time scales of our interest (order of 100 years), it can be treated safely as a linear trend.

[42] The study of the net global energy balances relies on the analysis of the statistical properties of the mean values and the interannual variabilities of the yearly time series $\langle\{B_\Omega\}\rangle_j$. The estimate of the yearly average of the net energy balance is computed as the mean over N years, and the estimate of the interannual variability is evaluated as the usual standard deviation of the time series. In the case of nonstationary time series, a linear trend has been removed before computing the standard deviation.

[43] Since we are interested in the statistical properties of the climatology, we need to compute the range of uncertainty of the estimates. In each case, the statistical properties of the mean and of the interannual average have been obtained by applying the standard block bootstrap resampling technique [*Wilks*, 2005; *Lucarini et al.*, 2006], where the resampling block has been chosen to be as long as the decorrelation time of the yearly time series. The 95% confidence interval has then been computed using a set of 1000 synthetic time series. Again, in the case of nonstationary time series, a linear trend has been removed before applying the block bootstrap resampling.

[44] As expected, the lagged correlation of the yearly time series of the net atmospheric and land energy balances becomes statistically nonsignificant as soon as the lag is larger than 1 year. Since the relaxation time of these subdomains is fast, no significant trend has been found in the SRESA1B scenario data either. Instead, the net climatic and oceanic balance time series feature a decorrelation time of the order of 5 years. Note that this is a simple way to see that the decadal climatic signals are mainly due to the ocean.

[45] In all cases, we find that the confidence intervals found with the block bootstrap method agree very well with the asymptotic (for $N \gg 1$) results. The asymptotic theory says that in the case of decorrelated time series, the standard deviation of the best unbiased estimate of the yearly average is approximately given by the interannual variability times the factor $2/\sqrt{N}$, while, in general, when a decorrelation time n is present, the factor is approximately $2\sqrt{n}/\sqrt{N}$, which is still $\ll 1$ if $N \gg n$ (as in our cases). The standard deviation of the best unbiased estimate of the interannual variability is a factor of $\sqrt{2}$ smaller than that of the corresponding mean.

[46] The investigation of the meridional transport in the preindustrial and SRESA1B scenarios is based on the
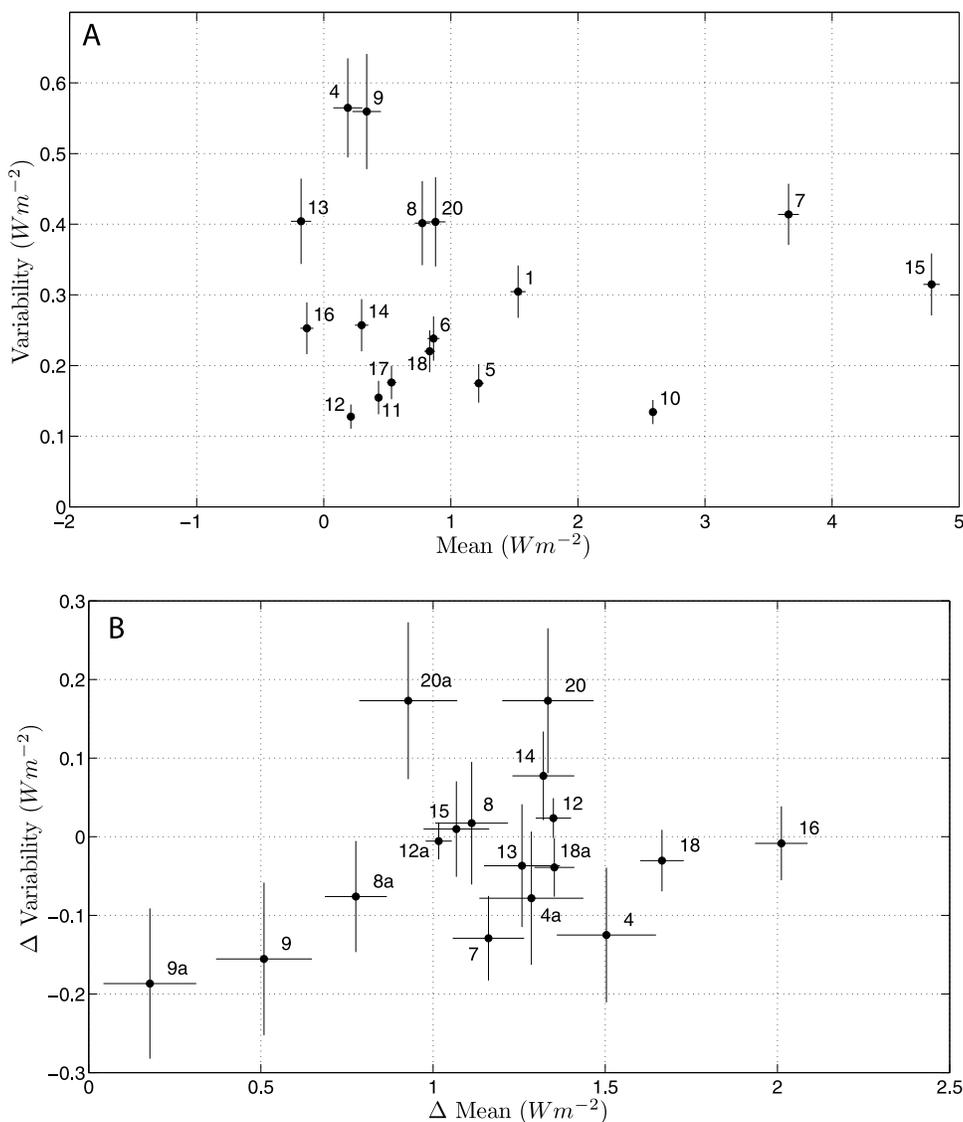
Figure 2. (a) Mean and standard deviation of globally averaged climate energy balance for all the models over 100 year long time periods in the preindustrial scenario. (b) Difference between the SRESA1B and the preindustrial scenario.

analysis of the time series of the one-dimensional fields $\langle T_\Omega(\varphi) \rangle_j$. The best unbiased estimator of the yearly average of the meridional transport is computed as the average of the N transport profiles obtained for each year, and the best unbiased estimate of the interannual variability has been evaluated as the usual standard deviation computed for each latitude. Again, trends have been removed when computing the standard deviation. Since when analyzing the meridional transport we are not testing a zero hypothesis, as in the case of the net global energy balances, we are less interested in obtaining detailed confidence intervals of our best estimates. Moreover, as we are dealing with 1-D fields with obvious spatial correlation, the applicability of the above mentioned block bootstrap resampling technique is more problematic. Therefore, we will present conservative estimates of the uncertainties by using the standard deviation of the time series as a proxy of the uncertainty of the best estimate of

the mean. As we shall see in section 4, the resulting interannual variability is so small that no piece of information will be lost with this procedure.

4. DIAGNOSTICS OF THE CLIMATE MODELS

4.1. Net Global Energy Balance

[47] Results are presented in terms of intensive quantities, so that the net CS (Figure 2) and atmosphere (Figure 3) energy balances are divided by the total surface of the planet, whereas the net ocean (Figure 4) and land (Figure 5) balances are divided by the total ocean and land surfaces, respectively. We wish to underline that the approach of studying surface energy fluxes is thermodynamically equivalent to, and computationally much more efficient than, analyzing the variations of the total energy of the geophysical fluids. The latter approach is quite unfeasible when an extensive CMs
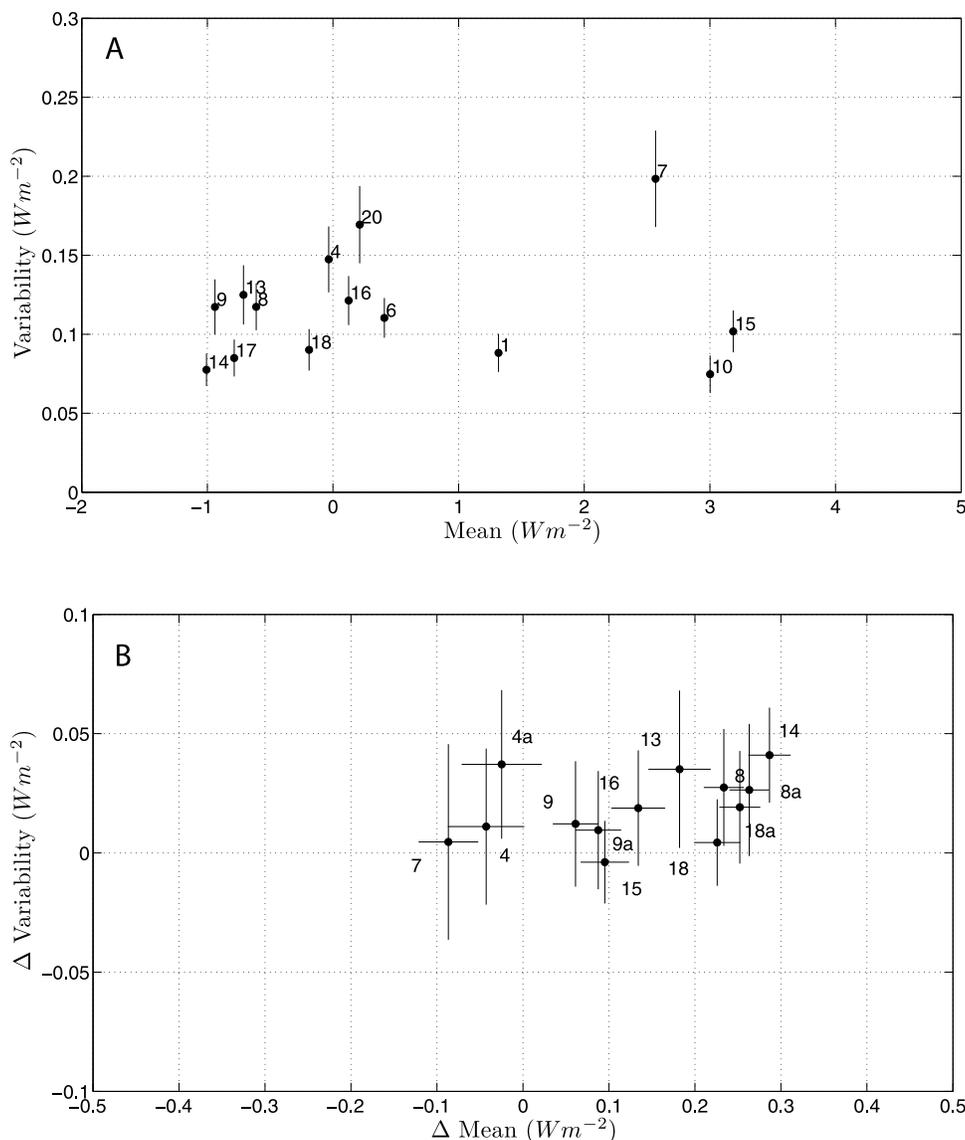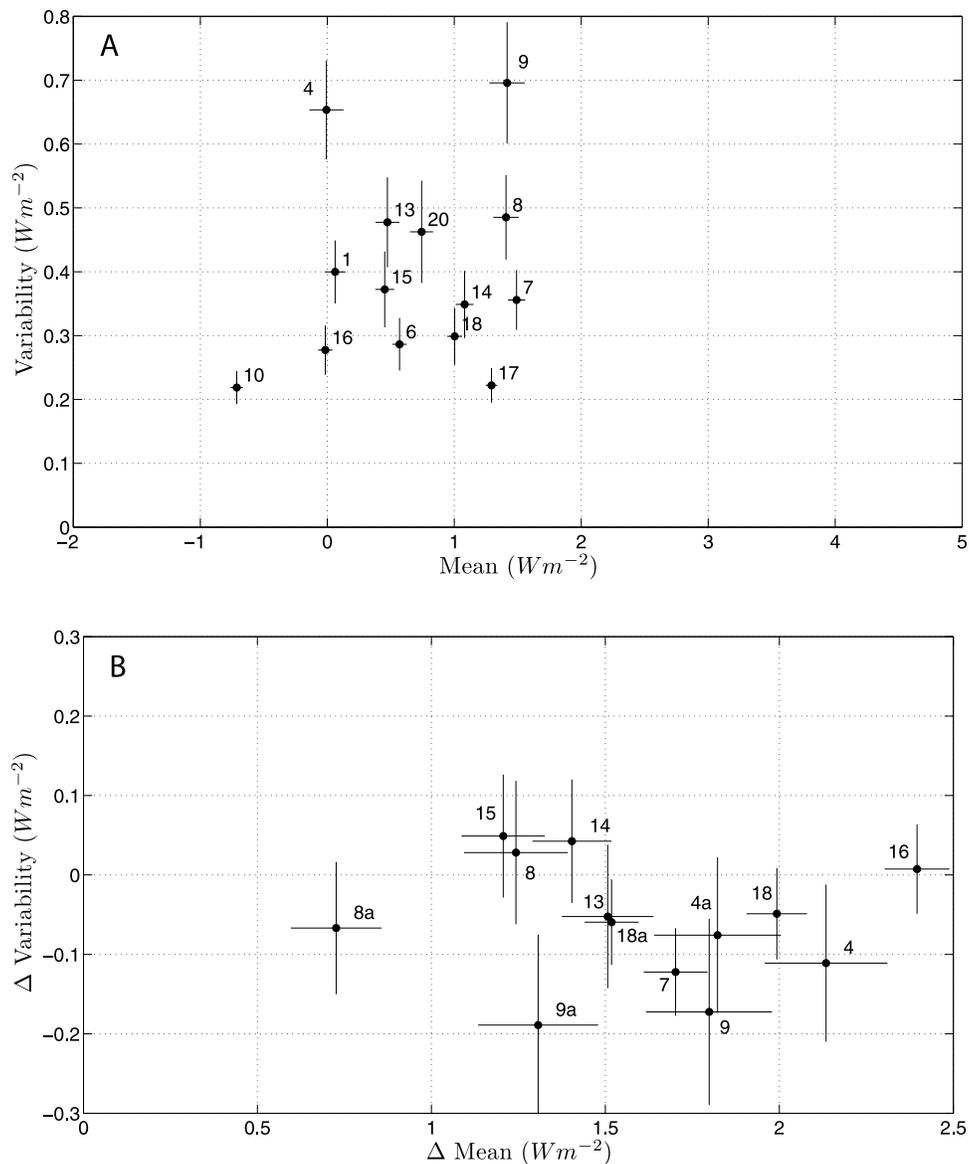
Figure 3. (a) Mean and standard deviation of globally averaged atmosphere energy balance for all the models over 100 year long time periods in the preindustrial scenario. (b) Difference between the SRESA1B and the preindustrial scenario. Numbers followed by "a" indicate data relative to the 23rd century in the SRESA1B scenario.

intercomparison analysis is performed because it would require the analysis of three-dimensional time-dependent fields for each CM.

[48] For each domain, we present in Figures 2a, 3a, 4a, and 5a the scatterplots of the 95% confidence interval of the mean value and of the standard deviation of the yearly averaged intensive energy balance in preindustrial conditions. In Figures 2b, 3b, 4b, and 5b, we also present a scatterplot of the 95% confidence interval of the variations of the mean value and the standard deviation from preindustrial to climate change conditions. The values have been obtained with the block bootstrap technique using 100 year long time series, selecting as a general rule the last 100 years of the data available in the data sets. In the case of SRESA1B simulations, we have considered the 2101–2200 data and, when available, the data referring to the 23rd century. The

95% confidence intervals have been centered on the best unbiased statistical estimators, and their half-width has been computed as twice the corresponding standard deviation computed as described in section 3.

[49] An immediate outlook on the problem of simulating physically sensible statistical properties of the net energy balance is given in Figure 1b, where we present the yearly time series (after application of a smoothing filter of 5 years for purely graphical reasons) of the TOA globally averaged net energy balance for the GFDL2.1 model (CM 9), which provides a good example for the generic behavior of the CMs. The preindustrial control run is depicted with the black line. The run performed under varying CO_2 concentrations is depicted with the red line. This run encompasses the 20th century simulation (starting in 1861 from year 41 of the time series of the preindustrial run
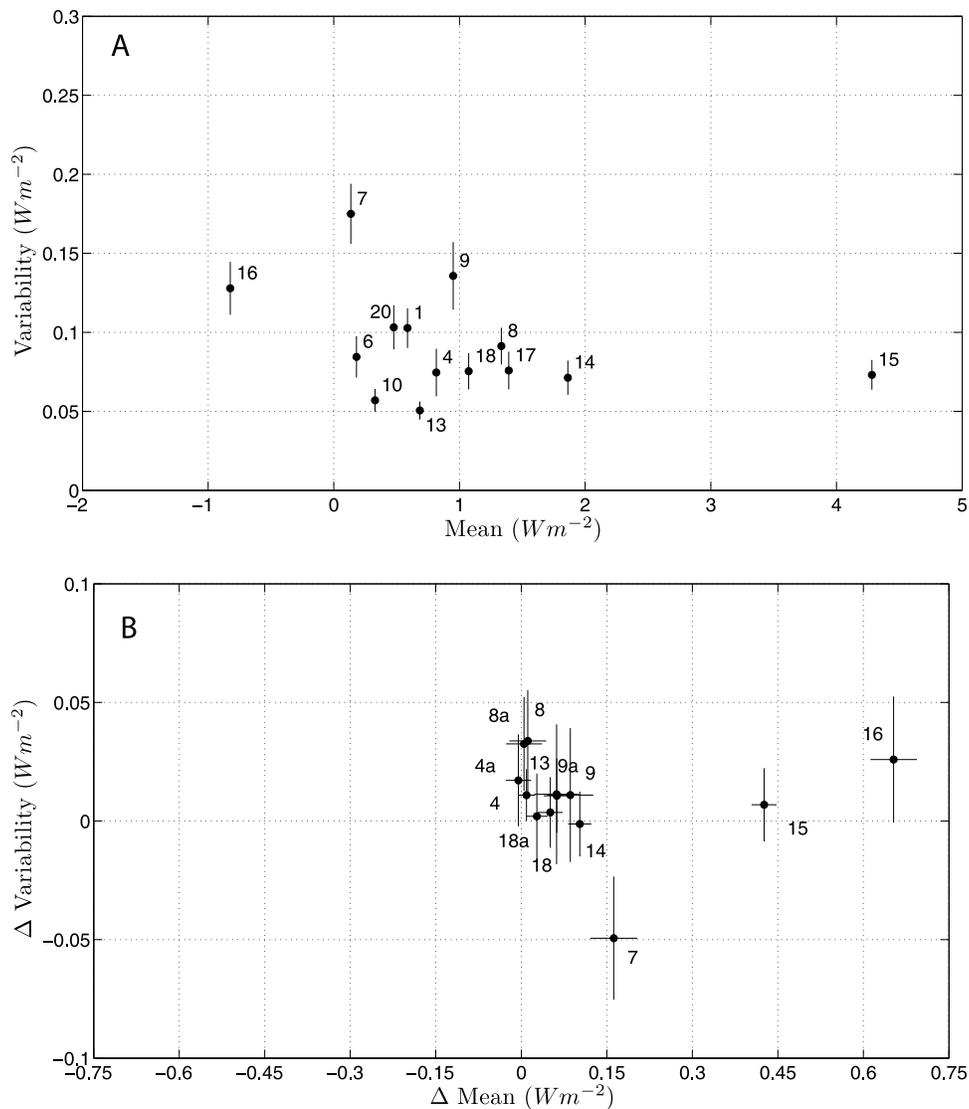
Figure 4. (a) Mean and standard deviation of globally averaged ocean energy balance for all the models over 100 year long time periods in the preindustrial scenario. (b) Difference between the SRESA1B and the preindustrial scenario. Numbers followed by "a" indicate data relative to the 23rd century in the SRE-SA1B scenario.

provided in the PCMDI CMIP3 data set) and the 21st century portion of the SRESA1B simulations (starting from the end of the 20th century simulation). Finally, the blue line depicts the 22nd and 23rd century SRESA1B run, where the CO_2 concentration is held fixed at 720 ppm. The energy balance of the unperturbed control run is biased toward a positive value of about 0.5 W m^{-2}. After the net energy balance increases as a result of the genuine heating related to the enhanced greenhouse effect due to increasing CO_2 concentration, the net energy balance decreases toward smaller values as the system relaxes toward the newly established steady state. The relaxation process occurs over a time scale of few centuries (not well resolved by the data) and can be safely attributed to the adjusting process of ocean state. Moreover, it is not clear whether the final

net energy balance bias will be analogous to the one the CM features in preindustrial conditions. Therefore, following the argument proposed when discussing Figure 1, it is, in principle, not trivial at all to estimate the actual net total heating of the planet due to the transition from 280 to 720 ppm CO_2 concentration.

4.1.1. Preindustrial Scenario

[50] In preindustrial conditions, most CMs feature a positive TOA yearly averaged net energy balance, and in not even one CM does the confidence interval intersect zero (see Figure 2a). Therefore, we can say that all CMs have a spurious behavior, which is apparently not compatible with steady state conditions. This is not the result of an adjustment in process since trends are wholly negligible but is instead a real bias. Therefore, none of the CMs seem to conform to the

Figure 5. (a) Mean and standard deviation of globally averaged land energy balance for all the models over 100 year long time periods in the preindustrial scenario. (b) Difference between the SRESA1B and the preindustrial scenario. Numbers followed by "a" indicate data relative to the 23rd century in the SRESA1B scenario.

idealized behavior depicted in Figure 1a. The imbalance is typically below 2 W m^{-2} in absolute value, apart from three outliers (CMs 7, 10, and 15) featuring positive imbalances ranging between 2.5 and 5 W m^{-2}. Models 4, 12, 13, 14, and 16 give the best performances as they feature biases smaller than about 0.2 W m^{-2} in absolute value. In principle, an average positive imbalance of 1 W m^{-2} at TOA, if no net flux across the land surface and the ocean bottom occurs, is consistent with a drift of the energy content of the fluid envelope of the planet of about 1.6×10^{22} J yr^{-1}.

[51] Very large discrepancies exist among CMs in the interannual variability of net energy balance since the computed standard deviations of the CMs' yearly net energy balances range between 0.1 and 0.6 W m^{-2}, with typical values of about 0.3 W m^{-2}. The presence of such a wide span of results requires some attention as it suggests the existence of intermodel differences in the intensity and/or

time scales of the negative feedbacks regulating the establishment of an (approximate) energy balance over multiyear time scales. We find no obvious relation between the estimates of the interannual variability and of the average energy imbalance.

[52] In order to disentangle the possible causes for the presence of global energy imbalances, the net energy balances of the atmosphere, of the ocean, and of land need to be analyzed in each CM. Common sense would suggest that under the hypothesis that the CM is energetically consistent, TOA spurious energy imbalances are basically due to biases in the surface net energy balance of an ocean still not close enough to steady state. Under this hypothesis, we should have virtually vanishing energy imbalances of the atmosphere and of the land components as they are thin components of the CS and they are quasi steady state.

[53] What we find instead is that the energy imbalances of the atmosphere (Figure 3) and land (Figure 5) are of the same order of magnitude as the bias of the energy imbalance of the ocean (Figure 4). Therefore, it seems physically unreasonable to interpret the imbalances of the CS as a whole and of its subdomains as being only (or mainly) due to still persistent transient conditions. Note that an imbalance of 1 W m^{-2} for the atmosphere corresponds to a staggering drift of about 3 K yr^{-1} of its average temperature. Since this is obviously not observed in the data, it is clear that the net energy balance of the CMs cannot be explained as a byproduct of the fact that the ocean component has not reached a true steady state. Therefore, some fundamental issues in the dynamics of the CMs need to be addressed.

[54] An explanation for the energy imbalance of the atmosphere can be tracked back to the lack of closure of the Lorenz energy cycle [*Lorenz*, 1955, 1967]. In fact, CMs, in general, do not have a detailed parameterization scheme for the reintroduction as thermal forcing of the energy dissipated by viscous dissipation, interaction with the boundary layer, cloud processes, and diffusion. For a specific study in this direction please refer to *Becker* [2003], while an example of prototypical value is given by *Lucarini and Fraedrich* [2009]. If in the considered medium the kinetic energy is just lost by dissipation and not reinjected in the system as heat (as also in the simple case of Boussinesq approximation), we expect a compensating spurious positive energy imbalance, which then does not translate into a temperature drift of the atmosphere but rather compensates a "ghost" energy loss and keeps the system at steady state.

[55] Land modules typically feature positive energy imbalances, whereas in steady state conditions the land component of CMs should see, when long-term averages are considered, a vanishing energy balance not only in the global mean but also in each grid point since no compensating horizontal transport is possible in a solid medium. Therefore, land modules must feature spurious water imbalances in the land climate modules [*Lucarini et al.*, 2008] due to, e.g., relaxation schemes in the bottom boundary conditions. Otherwise, they must present biases in the treatment of phase transitions, such as those related to the common procedure of calving ice and snow accumulating beyond given thresholds, as done, e.g., by *Lucarini and Russell* [2002] and *Trenberth and Fasullo* [2010a].

[56] The energy balance of the atmosphere (and, in principle, also of the ocean where, actually, some contribution from a slow temperature drift cannot be ruled out) in the majority of CMs is positive, thus suggesting that typically, there is an underestimation of the thermal energy produced at the end of the turbulent cascade dissipating the kinetic energy. Additionally, most land modules also feature a positive imbalance, suggesting that energy is lost because of inconsistencies in the treatment of phase transitions and water and heat fluxes.

[57] In all CMs the standard deviation of the annual net energy balance time series is much smaller for the land and atmosphere components than for the oceanic component, whose interannual variability is similar to that of the net

TOA balance. This confirms that the ocean acts as an integrator and plays a major role in controlling the variability of the net global energy balance over multiannual time scales.

[58] The performance of the various CMs wildly differs from case to case, and typically, for a given model, the quality of the representation of the net energy balance of the various subdomains is not consistent, thus pointing to the modular structure of the CMs. In any case, it should be noted that the biases we find for the atmosphere and ocean subdomains are at least 1 order of magnitude larger than the mechanical energy transfer term we have neglected, which implies that our approximation is consistent with the scope of our analysis.

[59] We hereby highlight some specifically interesting features. We first note that CMs 4 and 16 feature an energy balance of the atmosphere and of the ocean accurately close to 0, with the land modules introducing only a minor bias in the net global energy balance. As opposed to that, CM 7 features a well-balanced land component, but both the atmosphere and the ocean feature strong positive biases, indicating that the energetics of the fluid media require attention. On the other hand, the excellent performance on the net global balance of CM 14 comes from nonnegligible compensating errors in the sea, atmosphere, and land modules. The poor performance of CM 15 in terms of net global energy balance seems to derive from inconsistencies in the representation of the atmospheric and of the land energy balance. Energy inconsistencies in the atmosphere seem to be very relevant also for CM 1 and CM 10. Quite interestingly, in the case of CM 9 a net global energy balance close to 0 results from an almost perfect cancelation of the atmospheric and oceanic biases.

4.1.2. SRESA1B Scenario

[60] While for each CM it is crucial to assess the energy bias in the preindustrial, steady state conditions, globally and in each subdomain, it is also important to understand how the net energy balance changes as a result of a prolonged radiative forcing. The changes in the net energy balance between the preindustrial and the SRESA1B scenario are presented in Figures 2b, 3b, 4b, and 5b. Values are shown for data referring to 2101–2200 (just numerical index) and, where available, also to 2201–2300 (same numerical index with lower index "a").

[61] In the SRESA1B simulations most CMs feature an increase in the total energy imbalance, ranging from about 0.2 to 2.0 W m^{-2} with a typical value of about 1.0 W m^{-2}. This can be interpreted as the fact that the system is still gaining energy from outside as steady state conditions have not yet been attained. The relaxation process in action is made more evident by the fact that the change in the energy bias for the 23rd century is 20%–30% smaller than that for the 22nd century for all CMs where longer integrations are available (CMs 4, 8, 9, 12, 18, and 20). Note also that the changes shown in Figure 2b, which should be taken as robust signatures of climate change, are of the same order of magnitude or even larger than the biases found in steady state conditions (see Figure 2a).

[62] Disentangling this dependence of the imbalance on the climate state among the various subdomains provides additional insights (Figures 3b, 4b, and 5b). We find that the changes in the energy imbalance of the atmosphere are relatively small, ranging for all CMs between −0.1 and 0.3 W m^{-2}. This is consistent with the atmosphere being in a quasi steady state and supports the fact that the biases observed in preindustrial conditions are due to the internal dynamical processes and are relatively state independent.

[63] Similarly, for almost all models the net land energy balance changes by a small amount (less than 0.2 W m^{-2}, except for CMs 15 and 16) between SRESA1B and preindustrial conditions, again according to what is to be expected from a thin, fast system. Also in this case, the imbalances seem to depend weakly on the climate state. This provides further support to our hypothesis that the discrepancies found in the preindustrial case are, as for the atmosphere, related to the structure of the land modules.

[64] On the contrary, the ocean acts as a heat "reservoir" for all CMs: the net energy balance of the ocean consistently increases for all of the CMs by between 0.5 and 2.5 W m^{-2} in the SRESA1B scenario with respect to the preindustrial one, and it is the key player in determining the change in the net global balance shown in Figure 2. Note that values reported in Figure 4b are larger than those given for the TOA in Figure 2b because the ocean covers about 70% of the Earth surface: the extensive values of the change in the energy uptake are, instead, rather similar. The ocean is still relaxing to its steady state and is genuinely taking up heat. The relaxation to the steady state is confirmed by the fact that as for the net TOA energy balance, the values referring to the 23rd century are smaller than those referring to the earlier century by about 20%–30%.

[65] The importance of discussing the net energy balances for each subdomain separately can be further emphasized by the following argument. By checking only Figure 2a, we would conclude that there is a relatively large group of CMs (e.g., 4, 9, 11, 12, 13, 14, 16, and 17) featuring comparable performances in correctly representing the steady state properties of the CS. The analysis of Figure 2b does not allow us to discriminate among them as we know that a nonzero response has to be expected. Instead, we observe that CMs 4 and 16 consistently provide among the smallest energy imbalances of all subdomains in preindustrial conditions *and* also feature very small changes in the bias for the atmosphere and land components in SRESA1B conditions, as theoretically expected since these are thin subsystems. Therefore, we conclude that these CM are the best in terms of consistently representing the net energy balance of the CS. Unfortunately, we do not have enough data to assess the quality of CMs 11, 12, and 14 in all subdomains.

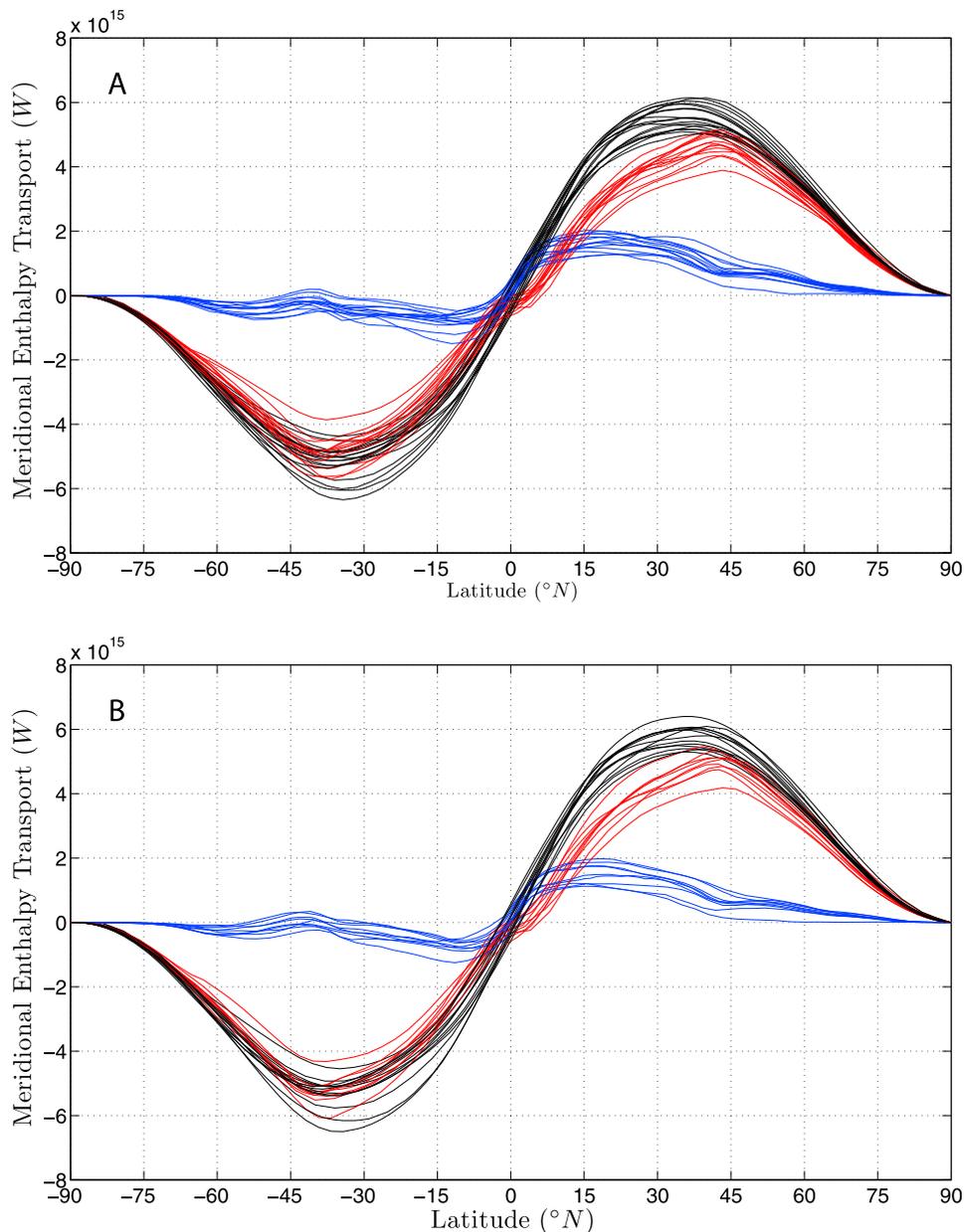## 4.2. Meridional Enthalpy Transport

[66] Plots of the time-averaged meridional enthalpy transport profiles obtained for the CMs analyzed in this study are shown in Figure 6a for preindustrial and in Figure 6b for SRESA1B conditions, where individual CMs results

are not singled out. All CMs feature a very low interannual variability on the meridional transport profiles, with absolute values of the local coefficients of variation (ratio of the standard deviation and of the mean) of the order of 1%, except near the region where meridional transport changes sign. Therefore, we will not analyze further the variability of the meridional transport but rather concentrate on its climatology. In each scenario, CMs agree on the most important features of the meridional transport, at least qualitatively, and no radical differences emerge between the two scenarios. This shows that the impact of the (substantial) CO_2 increase is to modulate the global circulation and not to disrupt it. We clearly see that the fluid envelope transports enthalpy from the low- to the high-latitude regions, with the effect of decreasing the meridional temperature gradient and of producing entropy [*Peixoto and Oort*, 1992; *Ozawa et al.*, 2003].

[67] In both scenarios, for most CMs the atmospheric enthalpy transport is, in agreement with today's climate [*Peixoto and Oort*, 1992; *Trenberth and Caron*, 2001; *Dell'Aquila et al.*, 2007], stronger in the Southern Hemisphere than in the Northern Hemisphere. In both hemispheres the peak of the atmospheric transport is located at the midlatitudes, where we have the maximum of the baroclinic activity. Most CMs feature a slight southward atmospheric transport across the equator, probably due to the fact that the Hadley cell is not perfectly symmetric since the intertropical convergence zone is located north of the equator [*Philander et al.*, 1996]. The atmospheric transport profile is very smooth, thus showing a strong dynamical link between the Hadley circulation and the midlatitude atmospheric variability [*Trenberth and Stepaniak*, 2003].

[68] The ocean features a strongly asymmetric meridional transport, which mirrors the asymmetry in the oceanic circulation between the Southern and the Northern Hemisphere [*Kuhlbrodt et al.*, 2007]. In both hemispheres most CMs feature two local maxima of transport, corresponding to the gyres. The larger one peaks in the low latitudes, while the secondary one peaks in middle to high latitudes. Overall, transport is stronger in Northern Hemisphere, with vanishing or weak northward cross-equatorial transport. The structure of the (weaker) meridional transport in the Southern Hemisphere is somewhat more complex as some CMs feature latitudinal bands of oceanic equatorward countertransport. As discussed by *Trenberth and Fasullo* [2010a], the representation of ocean transport in the Southern Hemisphere is a problematic aspect of most PCMDI CMIP3 CMs.

[69] Finally, the total northward transport is almost hemispherically specular, featuring a very smooth shape, not exactly vanishing at the equator for most CMs. Since the peaks of the atmospheric and of the oceanic transport are shifted by more than 20° and the atmospheric transport is typically stronger by a factor of ~3–5, the peak of the total transport is slightly shifted equatorward with respect to the atmospheric one. The most relevant qualitative feature of the meridional transport profiles presented in Figures 6a and 6b match remarkably well with those inferred from observa-
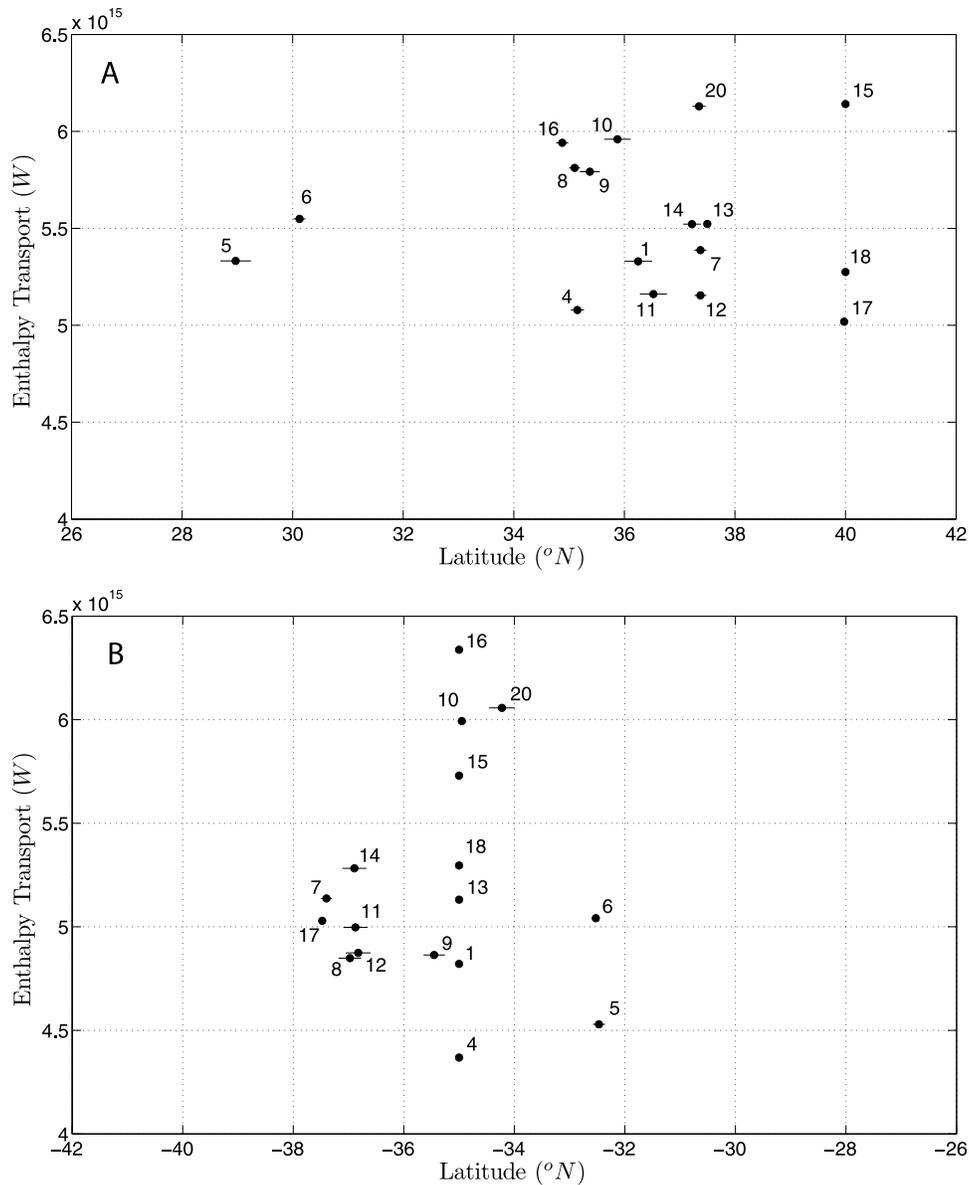
Figure 6. Mean total meridional enthalpy transport by the climate system (black lines), the atmosphere (red lines), and the ocean (blue lines) in (a) the preindustrial scenario and (b) the SRESA1B scenario for the 22nd century for all models where suitable data are available.

tions of the present net energy balance at TOA and at the surface [*Trenberth and Caron*, 2001], thus implying that they constitute robust structural properties of the CS which are relatively well captured by the CMs. Quite reassuringly, in agreement with the theoretical findings by *Stone* [1978b], for all CMs the total transport profile is remarkably similar in the two hemispheres in spite of wide differences in the contributions provided by transient and stationary waves in the atmosphere and by oceanic transport.

[70] From a quantitative point of view, the disagreements among CMs are large. In the preindustrial simulations, total and atmospheric transport features discrepancies among CMs up to 10% in the Northern Hemisphere and up to 20% in the Southern Hemisphere. Agreement is worse for the oceanic transport, with discrepancies being up to 40%–50% in the Northern Hemisphere. In the Southern Hemisphere, where the intensity of the oceanic transport is lower, we have discrepancies up to 100%; also, the qualitative behavior is less consistently represented [*Trenberth and Fasullo*, 2010a]. In the SRESA1B simulations the situation is rather similar, with the notable difference that even if the number of models included in the analysis is smaller, the model discrepancies on the ocean meridional transport are larger, probably as a result of the fact that transient time response of the ocean to CO_2 is rather uncertain.
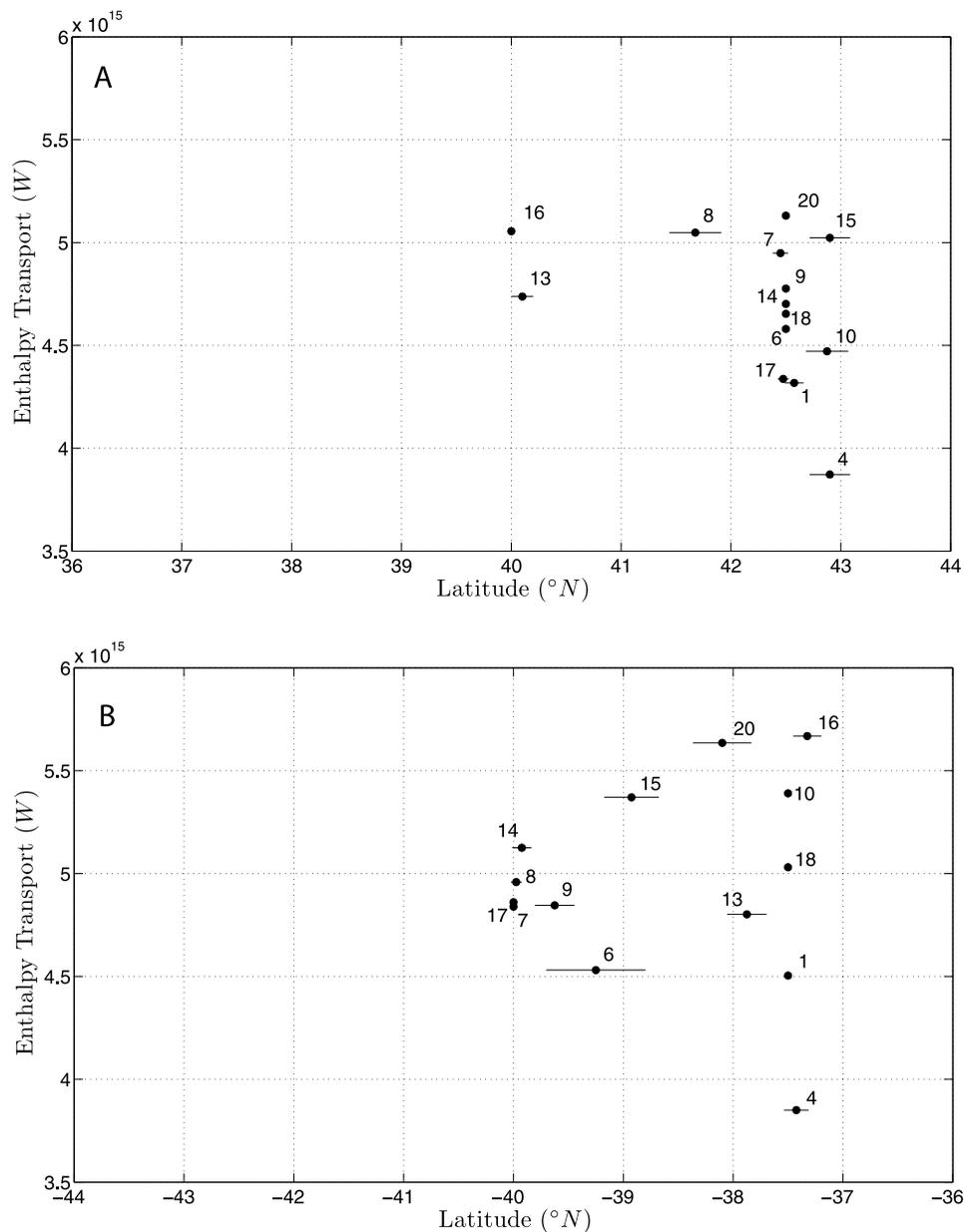
Figure 7. Value and position of the peak of the total poleward meridional enthalpy transport in the pre-industrial scenario (a) for the Northern Hemisphere and (b) for the Southern Hemisphere.

[71] Efficient metrics for the evaluation of CMs require the definition of simple but comprehensive indicators able to characterize the main features of the process under investigation. As an example, in a previous work we scaled down the Hayashi spectral density of midlatitude waves to some integrated variables describing the overall spectral weight of qualitatively different waves [*Lucarini et al.*, 2007]. In this case, we define a procedure to extract from the 1-D fields of meridional transports the essential information. Hence, from each yearly averaged transport profile $\langle T_\Omega(\varphi) \rangle_j$ we extract four variables, namely, the value of the peak of the northward transport in the Northern Hemisphere $\langle T_\Omega^{NH} \rangle_j$, its latitude $\langle \varphi_\Omega^{NH} \rangle_j$, the peak of the southward transport in the Southern Hemisphere $\langle T_\Omega^{SH} \rangle_j$, and its latitude $\langle \varphi_\Omega^{SH} \rangle_j$. The latitudinal band between $\langle \varphi_\Omega^{SH} \rangle_j$ and $\langle \varphi_\Omega^{NH} \rangle_j$ defines the region within Ω from which a net export of enthalpy is realized (except in the case of Southern Hemisphere oceanic equatorward countertransport), whereas $\langle T_\Omega^{NH} \rangle_j$ ($\langle T_\Omega^{SH} \rangle_j$) describes the total imbalance in the domain Ω north of (south of) $\langle \varphi_\Omega^{NH} \rangle_j$ ($\langle \varphi_\Omega^{SH} \rangle_j$).

[72] The various CMs feature rather different horizontal grids, in terms of resolution and structure (e.g., regular latitude-longitude versus Gaussian grids), so that the comparison of local indicators like those introduced above requires the remapping of all profiles $\langle T_\Omega(\varphi) \rangle_j$ into the same latitudinal grid. Therefore, we have selected the regular 2.5° spacing from −90°N to 90°N as a common framework since it approximately corresponds to the average resolution of the CMs and performed the remapping for all CMs using a linear interpolator. Results are robust with respect to the interpolating algorithm.
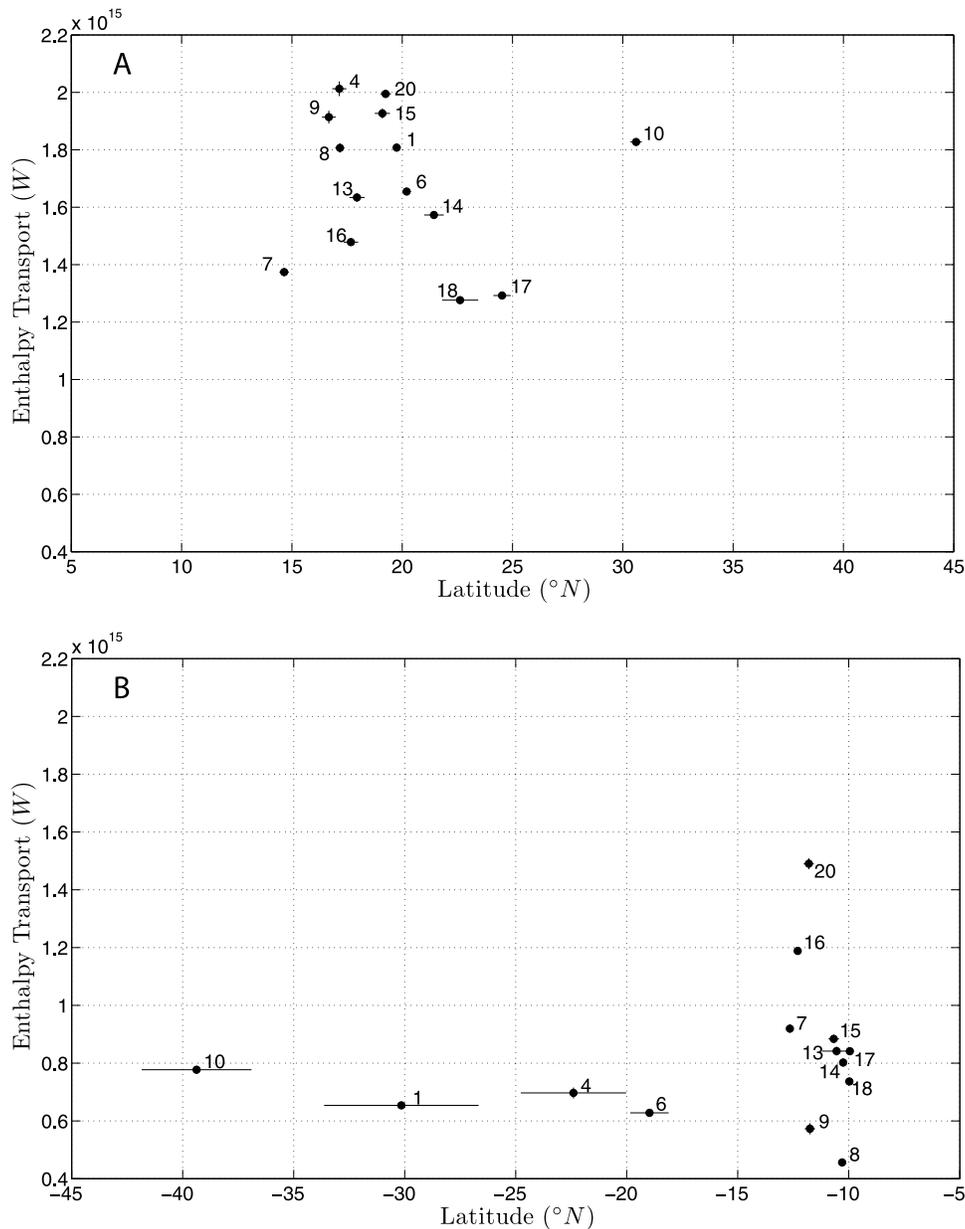
Figure 8. Value and position of the peak of the poleward meridional enthalpy atmospheric transport in the preindustrial scenario (a) for the Northern Hemisphere and (b) for the Southern Hemisphere.

4.2.1. Preindustrial Scenario

[73] We begin our analysis by focusing on the peaks of the total meridional transport in preindustrial conditions for the Northern and Southern Hemispheres, depicted in Figures 7a and 7b, respectively. We first observe that in both hemispheres for most CMs the total meridional transport peaks at 5–6 PW (1 PW = 10^{15} W), with an effective range of about 20% and with maxima situated between 34° and 38°. Therefore, all CMs feature an average positive TOA imbalance in the tropical regions of about 40 W m^{-2}, accompanied by a compensating negative budget in the mid-high latitudes. On average, the total transport in the Southern Hemisphere is typically slightly smaller by about 0.3 PW, in agreement with what was found by *Trenberth and Fasullo* [2010a] for present cli-

mate conditions on a similar set of CMs. The model-wise disagreements on the localization of the transport maxima are more serious in the Northern Hemisphere, while disagreements on the peak value of the transport are somewhat wider in the Southern Hemisphere.

[74] For each CM, the interannual variability of the position and the strength of the transport maximum is very small, so that typically, each year the meridional transport peaks at the same grid point, and the transport maximum, as also discussed in the context of Figure 6a, has weak year-to-year variations. This is hardly unexpected since we are looking into one of the most robust features of the CS, which should be affected only by large climate fluctuations. We may guess that when the CS is close to a tipping point, the enhanced, large-scale, organized fluctuations also might

Figure 9. Value and position of the peak of the poleward meridional enthalpy ocean transport in the preindustrial scenario (a) for the Northern Hemisphere and (b) for the Southern Hemisphere.

heavily impact these indicators. An interesting result is that CMs tend to behave consistently in the two hemispheres. Typically, relatively strong (weak) transports are observed in both hemispheres, as in the case of CMs 10, 15, 16, and 20 (CMs 4, 5, 11, 12, and 17). Similarly, relative poleward (equatorward) anomalies in the position of the transport maxima are often consistent in the two hemispheres, as in the case of CM 17 (CMs 5 and 6).

[75] The agreement among CMs in the representation of the atmospheric enthalpy transport in the Northern (see Figure 8a) and Southern Hemispheres (see Figure 8b) is also problematic. In both hemispheres the agreement among CMs is rather good on the position of the maxima (within one grid point), with a slightly more poleward position of the maxima in the Northern than in the Southern Hemi-

sphere. Since we are dealing with latitudes of about 40°, we deduce that a great contribution to the transport is performed by baroclinic activity and that the position of the peak coincides with that of the storm track. As in the case of the total transport, the interannual variability of the position and the intensity of the peak of the atmospheric transport is very small for all CMs.

[76] Instead, quantitative differences in the intensity of the transport are quite pronounced in both hemispheres. In the Northern Hemisphere, most values are clustered within 1 PW around 4.7 PW, which means a spread of about 20%. Such inconsistencies in the representation of the large-scale properties of the atmosphere in the North- ern Hemisphere agree with what discussed by *Lucarini et al.* [2007]. In this paper, albeit referring to the present climate,
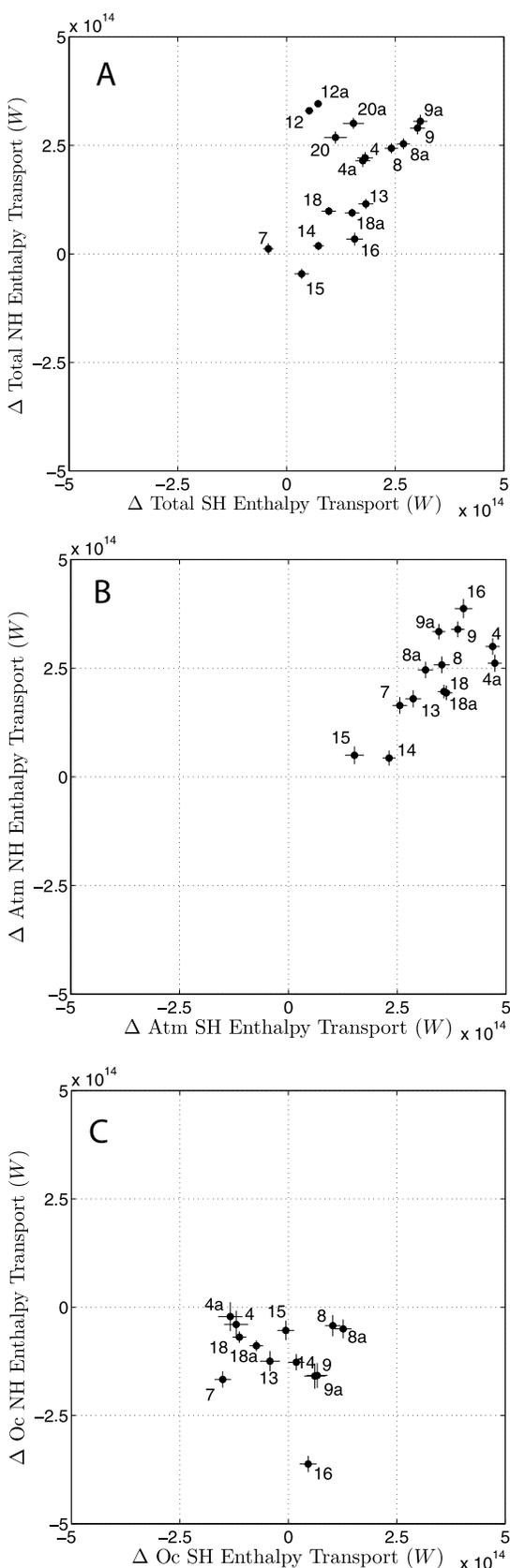
Figure 10. Difference in the peak value of the poleward meridional enthalpy transport for both hemispheres between the SRESA1B and the preindustrial simulations. Data are provided for (a) the total transport, (b) the atmospheric transport, and (c) the ocean transport.

it is shown that large discrepancies among PCMDI CMIP3 CMs exist in the representation of the Northern Hemisphere winter atmospheric variability in the midlatitudes, which is when and where the meridional energy transport is particularly effective.

[77] In the Southern Hemisphere, even if the total meridional enthalpy transport is typically lower, for most CMs the values of the maxima of the atmospheric transport tend to be somewhat larger than in the Northern Hemisphere, by up to 0.5 PW. This is in agreement with what was found by *Dell'Aquila et al.* [2005, 2007] for present climate data, and it is basically due to the stronger baroclinic activity in the Southern Hemisphere [*Trenberth*, 1991]. The intensity span among CMs is more pronounced than in the Northern Hemisphere, reaching a value of 1.5 PW (about 30%), thus suggesting more uncertainty among CMs in the representation of the meridional temperature gradient in the Southern Hemisphere. We also observe that some CMs feature extremely weak (CMs 1 and 4) and extremely strong (CMs 15, 16, and 20) atmospheric transports in both hemispheres, which hints at the presence of some peculiar structural properties of the atmospheric circulation.

[78] When looking at CMs' performances in terms of representation of the ocean meridional enthalpy transport, the picture is rather different than in the two previous cases. Results are reported in Figures 9a and 9b for the Northern and Southern Hemispheres, respectively. Our findings support the idea that the discrepancies among CMs in the representation of the ocean circulation, and especially that of the Southern Ocean, are much larger than in the case of atmospheric circulation.

[79] In preindustrial conditions, in the Northern Hemisphere the intensities of the maxima of the ocean transport are between 1.3 and 2 PW, so the span is about 40% of the typical value. The positions of the peaks are not correlated to their intensity and are distributed between 15°N and 25°N, with a span of four grid points. The maximum for CM 10 is relevantly shifted northward, up to around 30°N. For each CM, interannual variability is small for both intensity and position of the maximum, thus supporting the idea that the peak of the oceanic transport in the Northern Hemisphere provides a robust characterization of the state of the oceanic system.

[80] As already seen in Figure 6a, in the Southern Hemisphere the definition of the peak of the oceanic transport is more problematic because of the presence of two well-defined local maxima. For most CMs the peak of the oceanic transport is located in a relatively narrow band between 12.5°S and 10°S (one grid point span). On the contrary, CMs 1, 4, 6, and 10 feature a bimodality in the location of the maximum: in some years the maximum is located around 10°S, and in other years the maximum of the transport is realized around 55°S. Therefore, for these CMs, which are characterized by a weak oceanic transport, the average position of the peak is between these two latitudes, and the interannual variability is very large. In particular, the high-latitude peak is realized very often in CMs 1 and 10. A more detailed analysis of the distribution of the maxima
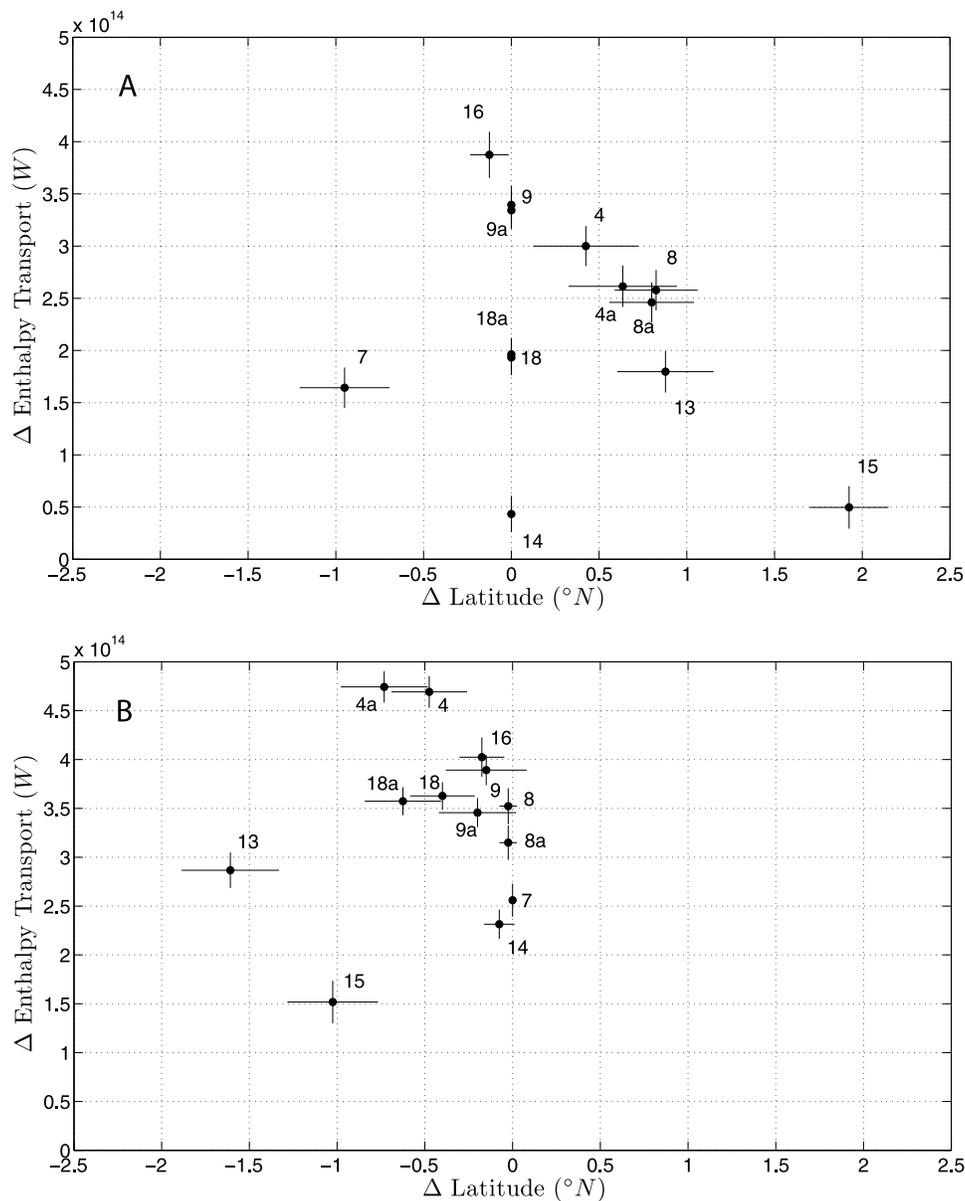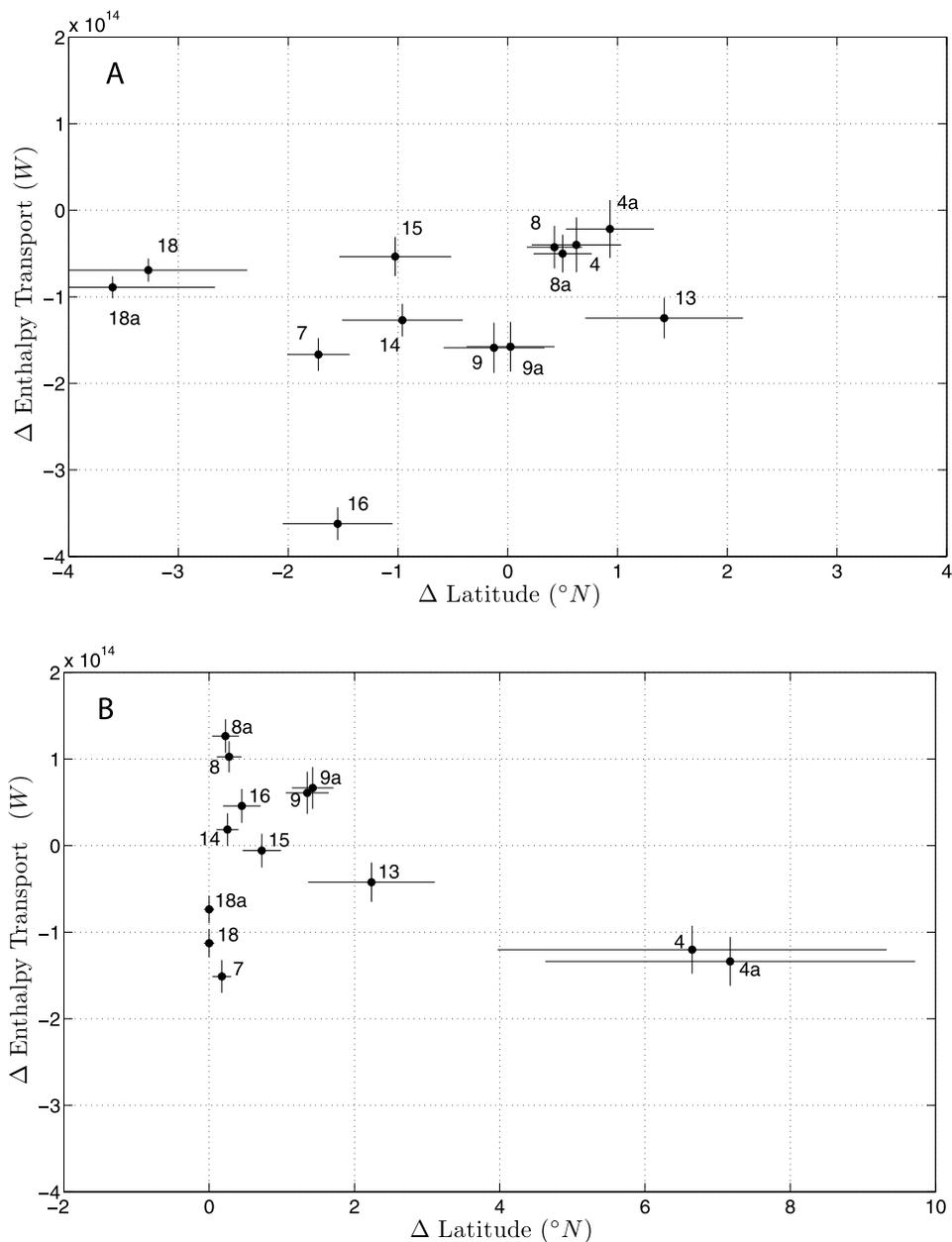
Figure 11. Difference in the value and position of the peak of the atmospheric poleward meridional enthalpy transport between the SRESA1B and the preindustrial simulations for the (a) Northern Hemisphere and (b) Southern Hemisphere.

accounting for the bimodality of the probability density function of the locations and the understanding of the physical reasons for and climatological implications of this property would surely be of interest. Restricting ourselves to the CMs with a clearly located maximum, we can see that the span of the intensities is very large. We observe values ranging from 0.4 to 1.6 PW, so that the span is about 100% of the typical value. Instead, for each CM, the interannual variability on the value and position of the peak is rather small. The existence of such discrepancies among the observed climatologies is in agreement with findings of previous studies, which showed that the PCMDI CMIP3 models feature marked difficulties in the representation of large-scale energy processes in the Southern Ocean [*Trenberth and Fasullo*, 2010a].

4.2.2. SRESA1B Scenario

[81] Rather interesting differences emerge when comparing the simulations performed with preindustrial scenarios and those performed with increased CO_2 concentration. The first nontrivial information is that for each CM the position of the peak of the total meridional transport does not change significantly, in both the Southern and the Northern Hemispheres. The shift is at most one grid point, and model-wise, no systematic (poleward or equatorward) variation is found (not shown). The behavior of each CM is in agreement with the results by *Stone* [1978b] on the stability of the position of the peak of the transport independently, e.g., of the specific atmospheric composition. Therefore, the latitudinal boundary separating the areas of the planet that differ on the sign of the difference between the incoming and outgoing

Figure 12. Difference in the value and position of the peak of the ocean poleward meridional enthalpy transport between the SRESA1B and the preindustrial simulations (a) for the Northern Hemisphere and (b) for the Southern Hemisphere.

radiation is rather stable with respect to changes in the CO_2 concentration.

[82] Changes in the intensity of the meridional transport are more interesting. In Figure 10a we plot the change in the value of the peak of the meridional transport in the Southern Hemisphere versus the change observed in the Northern Hemisphere. Note that in all cases the 95% confidence interval is very narrow. We find that most CMs feature positive variations in both hemispheres up to about 10% of the preindustrial value (typical changes range around 5%), which implies a more efficient energy redistribution in a warmer climate. This contributes to the mechanism of polar amplification [*Solomon et al.*, 2007] as its additional heat is

fed into the high-latitude regions of the globe. Given the smaller thermal inertia of the system, the effect in terms of surface temperature is expected to be stronger in the Northern Hemisphere. Instead, CMs 7, 14, and 15 foresee a negligible change in the meridional transport in both hemispheres, thus featuring a very stable climate.

[83] When looking at changes in the meridional atmospheric transport, we again find that in both hemispheres (see Figures 11a and 11b) changes in the position of the peak are small for all CMs but, with a few exceptions, systematically poleward. As the atmospheric transport peaks are related to baroclinic activity and storm track, this result seems to be (at least partially) in agreement with those found

TABLE 2. Correlation Between Annual Maxima of Atmospheric and Oceanic Poleward Transport in Each Hemisphere[a]

Model	PI-SH	PI-NH	SRESA1B-NH	SRESA1B-SH
1	−0.30	−0.14	–	–
2	–	–	–	–
3	–	–	–	–
4	−0.32	−0.29	−0.46	−0.42
5	–	–	–	–
6	−0.36	−0.26	–	–
7	−0.48	−0.20	−0.45	−0.20
8	+0.05	−0.34	−0.39	−0.37
9	−0.27	−0.35	−0.21	−0.12
10	−0.62	−0.36	–	–
11	–	–	–	–
12	–	–	–	–
13	−0.11	−0.09	−0.26	−0.21
14	−0.08	+0.01	−0.27	−0.24
15	−0.20	−0.46	−0.05	−0.28
16	−0.31	−0.33	−0.48	−0.43
17	−0.09	+0.15	–	–
18	−0.27	−0.17	−0.11	−0.08
19	–	–	–	–
20	−0.48	−0.15	–	–
21	–	–	–	–
22	–	–	–	–
23	–	–	–	–

[a]The 95% confidence interval width is ±0.20 in all cases. PI and SRESA1B (2101–2200) scenarios. PI, preindustrial; SH, Southern Hemisphere; NH, Northern Hemisphere.

by *Yin* [2005], who observed in 21st century climate simulations a poleward shift of the core of the midlatitude atmospheric variability, with a stronger signal in the Southern Hemisphere. Nonetheless, recent analyses have attributed the shift of the peak in the Southern Hemisphere to spurious trends in clouds cover [*Trenberth and Fasullo*, 2010a]. The impact of CO_2 increase is instead relevant when the values of the peaks of the atmospheric transport are considered. In Figure 10b we show that all CMs feature consistent increases (up to about 12%) of the atmospheric transport in both the Northern and the Southern (where changes are typically larger) Hemispheres, with the exception of CMs 14 and 15, which foresee only a negligible increase of the transport for the Northern Hemisphere. Our results agree with those shown by *Held and Soden* [2006], who presented aggregated results for the CMs' ensemble mean.

[84] The response of the ocean to CO_2 increase is also of great interest. We observe typical changes of the order of 0.1–0.2 PW (Figure 10c). These are large relative changes in the ocean transport, ranging from 10% to over 50%. Half of the CMs foresee a decrease in the transport in the Southern Hemisphere, while a decrease in the transport is foreseen for all CMs in the Northern Hemisphere. The observed (partial) compensation between the changes in the oceanic and atmospheric transports is in overall agreement with the aggregated results presented by *Held and Soden* [2006]. There is no obvious link between the observed changes and the unperturbed values. Instead, as shown in Figures 12a and 12b, in both hemispheres most CMs feature (usually small) equatorward shifts in the position of the maxima, of the order of half of a grid point. The largest equatorward

shifts are realized for CM 18 in the Northern Hemisphere and CM 4 in the Southern Hemisphere, which featured among the most poleward positions of the maxima in the preindustrial conditions.

4.2.3.   Atmosphere-Ocean Transport Compensation

[85] The Bjerknes compensation mechanism suggests a compensating role of the atmosphere and of the ocean in transporting heat poleward [*Bjerknes*, 1964]. The mechanism has been the subject of detailed studies also performed on PCMDI CMIP3 CMs [*Shaffrey and Sutton*, 2006; *van der Swaluw et al.*, 2007]. In section 4.2.2 we have seen that for higher CO_2 concentration for basically all CMs the increase in the atmospheric transport is moderated by the decrease in the oceanic transport in both hemispheres. We test here whether a hemispheric compensating mechanism is also in place on shorter time scales by computing for both hemispheres the linear correlation between the yearly time series of the maxima of the meridional transport for the atmosphere and for the ocean. Results are shown in Table 2. Note that the 95% confidence interval of the null hypothesis corresponds to that of an uncorrelated time series since the atmospheric transport has no memory. We find that no CM, in no scenario, in neither hemisphere features a statistically significant positive correlation between the two time series. Instead, we find that the majority of the CMs feature a statistically significant negative correlation between the time series in both hemispheres and in both scenarios. CMs 4, 6, 7, 10, 16, and 20 seem to have an especially strong and consistent compensation mechanism. We see that in both hemispheres the negative correlation is often reinforced in the SRESA1B scenario, suggesting that the mechanism may become stronger in a warmer climate. This may be motivated by the stronger coupling due to intensified (thanks to Clausius-Clapeyron relation) latent heat fluxes under global warming conditions. The fact that the Bjerknes compensation mechanism is active in both hemispheres and is also evident when yearly time series are considered further suggests that it acts at a local or regional scale. Indeed, if the compensation were related to large-scale ocean-atmosphere coupled processes, the behavior would be totally different in the two hemispheres, given the strong asymmetry of the oceanic circulation.

5.   SUMMARY AND DISCUSSION

[86] In this work we have tackled the problem of assessing the consistency of a large set of state-of-the-art CMs in their representation of the net energy balance of the whole CS as well as of its main subdomains (atmosphere, ocean, and land). Moreover, we have discussed the statistical properties of their meridional enthalpy transports due to atmospheric and oceanic motions.

[87] Our analysis has considered the preindustrial and SRESA1B simulations performed following the standards provided by the PCMDI CMIP3 project, which has greatly contributed to the redaction of the IPCC4AR [*Solomon et al.*, 2007]. The preindustrial scenario has played the role of a control run with fixed CO_2 concentration and has been

instrumental for defining a baseline for dealing with transient-free climate behavior and for setting the objects of our investigation in the well-defined context of the nonequilibrium steady state systems [*Gallavotti*, 2006]. The other scenario has been selected in order to understand how the energetics of the CS change as a result of changes in the CO_2 concentration.

[88] We find that in the preindustrial simulations no CMs are rigorously consistent with the condition of stationary state, so that in all cases a driftless state is obtained even if nonvanishing net energy balances are realized for the global climate as well as for its subdomains. The performances of the various CMs in terms of consistency of the representation of the net energy balances are wildly different.

[89] When global balances are considered, CM imbalances are positive in most cases, with values spanning between −0.2 and 2 W m^{-2}, with a few CMs featuring imbalances larger than 3 W m^{-2}. Typically, this behavior is interpreted as resulting almost entirely from biases in the net surface energy balance of an "energy-absorbing" ocean, which has not yet attained its steady state, with an ensuing almost unnoticeable spurious (but "harmless") drift in the climatological temperature, due to the ocean's large heat capacity. On the contrary, the energy imbalances in the land and atmospheric subdomain are of the same order of magnitude (about 1 W m^{-2}) as those of the ocean, which rules out the usual interpretation. Inconsistencies are mostly related to basic issues in the land and fluid modules of the CMs. Note that for some of the CMs (most notably CM 9) "good" net global balances result from compensating errors in the subdomains. Instead, CMs 4 and 16 perform consistently well in all subdomains, which suggests that their representation of global energy processes is more physically consistent.

[90] Most CMs feature spurious positive energy imbalance for the land subdomain, as a result of unphysical biases in water fluxes [*Lucarini et al.*, 2008] and in the treatment of phase transitions. As an example, long-term accumulation or loss of 15 mm yr^{-1} of liquid water (which amounts to about 1.5% of the intensity hydrological cycle) or 12 mm yr^{-1} of ice, e.g., due to spurious water infiltration or ice calving, correspond to an energy bias of about 1 W m^{-2} in absolute value.

[91] Most CMs feature spurious positive imbalances for the energy of the atmosphere, with biases of the order of 1 W m^{-2}. If such an imbalance were related to a genuine energy input to the atmospheric subsystem, it would correspond to a staggering average temperature trend of 3 K yr^{-1}. As such a trend is definitely not observed, the spurious energy imbalance must compensate an unphysical energy sink (if the imbalance if positive) or source (if the imbalance is negative). The inconsistency in the net energy balance of the atmosphere is mainly related to the fact that kinetic energy dissipated by various processes, including viscosity and diffusion, cloud parameterization, and interaction with the boundary layer, is not exactly reinjected in the system as thermal energy. This has been analyzed in detail by *Becker* [2003], whereas an example of prototypical value has been provided by *Lucarini and Fraedrich* [2009]. As an example,

commonly used hyperdiffusion schemes feature mathematical properties that make them inadequate in terms of correctly representing the net energy balance and introduce an artificial energy sink.

[92] These inconsistencies may have relevant impacts in the global properties of the atmospheric and of the oceanic circulation as they alter the input-output terms of the Lorenz energy cycle. Recently, using the intermediate complexity model Planet Simulator (PLASIM) [*Fraedrich et al.*, 2005], it has been proven that when the energetic inconsistencies of the fluid and of the land modules are fixed, the representation of the global energy balance is greatly improved, with an obtained reduction of the spurious imbalance by about 1 order of magnitude [*Lucarini et al.*, 2010a, 2010b].

[93] We can link the presence of a bias in the net global energy balance of the system ΔE to a bias ΔT_E in the radiative temperature T_E of the planet. Using a linear expansion to the blackbody relation, we find that $\Delta T_E/\Delta E = -1/(4\sigma T_E^3)$ (where σ is the Boltzmann constant), which gives ≈ -0.27 K W^{-1} m^2 using usual Earth values. Moreover, if we consider the simple but effective parameterization for the outgoing longwave radiation expressed as the linear relationship $A + BT_S$ with respect to the surface temperature T_S, we find that an energy bias ΔE is related to a surface temperature bias by $\Delta T_S/\Delta E = -1/B$. Using *Nakamura et al.*'s [1994] values, the resulting impact of the imbalance on the surface temperature is ~ -0.6 K W^{-1} m^{-2}). Therefore, we have that a positive (negative) imbalance, which actually "cures" an energy leakage (source) in steady state conditions, is related to a spurious cooling (warming) of the system, both in terms of its thermodynamic temperature and of its surface temperature. As CMs basically tend to have positive energy imbalances in preindustrial as well as in increased CO_2 conditions, we expect them to feature a cold bias. We believe this is an alternative way of rationalizing the long-standing problem of the cold bias of CMs attributed, instead, by *Johnson* [1997, 2000] to spurious entropy generation due to numerical noise under the condition of vanishing energy balances.

[94] Another surprising result worth mentioning is that the interannual variability of the net energy balances is model-wise very different, with values spanning almost an order of magnitude, both in the global case and when subdomains are considered. This calls for a detailed reexamination of the differences among the strengths of the feedbacks controlling the net energy balances in the various CMs.

[95] When looking at the net energy balances obtained with the SRESA1B scenario runs, we find that the atmosphere and the land imbalances change by a rather small amount (typically up to 0.2 W m^{-2}) with respect to the preindustrial runs. Since we are dealing with thin subsystems with small heat capacity, this suggests that the energy imbalance is not heavily climate dependent but actually related to deficiencies in the structure of the module. Instead, the ocean energy imbalance increases for all CMs, in agreement with the fact that in transient global warming conditions the water masses genuinely take up heat since the system is not yet at steady

state. It must be observed that the spread of the heat update is very large, going from about 0.2 to over 2 W m^{-2}. Such large discrepancies contribute to explaining the relatively large disagreements among the CMs in the simulated transient climate change at surface.

[96] The analysis of the inferred meridional enthalpy transports has provided us with a picture of how the CMs represent the process of reequilibration by which the fluid components of the CS decrease the temperature difference between the low- and high-latitude regions in both hemispheres. The qualitative agreement among the CMs is rather good, and the obtained meridional transport profiles resemble recent estimates obtained with observational data [*Trenberth and Caron*, 2001] and CMs' diagnostics studies [*Trenberth and Fasullo*, 2010a], thus confirming a fair representation of these structural properties of the CS.

[97] It is important to note that the indirect calculation of the transport is a linear operation since it involves the integration of the vertical fluxes of energy at the boundary of the fluid envelopes and at the TOA. Therefore, we need to consider only 2-D diagnostic fields with the temporal resolution of the climatology we wish to compute (yearly data, in this case). As opposed to that, the direct calculation of the transports requires 3-D diagnostic fields with high temporal resolution since quadratic quantities are involved. Therefore, our approach requires storage and processing costs smaller by orders of magnitude than what is needed with a direct calculation. While the indirect calculation is rigorously valid only if steady state conditions are precisely obeyed and the integrated energy balances are vanishing, the biases found in the CMs are small enough that only negligible errors are introduced [*Carissimo et al.*, 1985].

[98] Since we are dealing with 1-D fields, the necessity to consider simpler metrics has driven us to consider more manageable indicators. We have then analyzed the statistical properties of the intensities and positions of the hemispheric peaks of the atmospheric, of the oceanic, and of the total transport.

[99] In preindustrial conditions, we have found that the CMs do not agree precisely on the estimate of the total transport driven by the CS from the low- to the high-latitude regions as discrepancies of the order of 15%–20% around a typical value of about 5.5 PW (5.2 PW) are found in the Northern (Southern) Hemisphere. Recent studies have suggested that the PCMDI CMIP3 CMs might slightly underestimate the total transport in the Southern Hemisphere because too little radiation is absorbed in the tropical regions because of a cloud bias [*Trenberth and Fasullo*, 2010a]. When considering the atmospheric transport, we find that in the Northern Hemisphere the CMs feature discrepancies in the peak intensity of 15%–20% around a typical value of about 4.7 PW, whereas in the Southern Hemisphere the peaks of the transport are typically larger by about 0.5 PW, and the discrepancy among CMs is more evident. The agreement among CMs is much better for the atmospheric transport when looking at the positions of the peaks, with disagreements of only one grid point at most. The atmospheric transport peak is situated between 40°N and 43°N in the Northern Hemisphere and 37°S and 40°S in the Southern Hemisphere. The peak of the total transport is shifted equatorward in the Northern (Southern) Hemisphere by about 5° (3°), and the CM spread is somewhat larger. This confirms that in spite of the serious discrepancy in the mechanisms contributing to the meridional transport in the two hemispheres, the overall properties are very closely symmetric with respect to the equator. This is in excellent agreement with *Stone*'s [1978b] theoretical results. It is important to note that for each CM the interannual variability of the position and intensity of the transport maxima is very small, so that we are dealing with a very robust climatic feature.

[100] The intermodel uncertainties on the position of the peak of the total transport are mainly due to the large disagreements among CMs on the position of the peak of the ocean transport and on its intensity. Previous analyses have shown that the ability of PCMDI CMIP3 CMs in describing the ocean transport in the Southern Hemisphere is especially problematic [*Trenberth and Fasullo*, 2010a]. All CMs agree on the fact that the oceanic transport is smaller than the atmospheric transport in both hemispheres and that the oceanic transport in the Southern Hemisphere is much weaker than that in the Northern Hemisphere. Nevertheless, large quantitative inconsistencies emerge: the disagreements on its intensity are of the order of 50% in the Northern Hemisphere (with values ranging from about 1.3 to about 2.1 PW) and of the order of 100% in the Southern Hemisphere (with values ranging from about 0.4 to about 1.6 PW). All CMs agree that the peak of the oceanic transport is shifted equatorward with respect to the peak of the atmospheric transport in both hemispheres. Yet large quantitative disagreements exist on the actual positions of the peaks. In the Northern Hemisphere, for all CMs except CM 10, whose peak is shifted poleward, the ocean transport peaks between 15°N and 25°N. In the Southern Hemisphere, for most CMs the peak is typically situated between 10°S and 20°S, whereas CMs 1, 4, 6, and 10 feature a much more poleward shifted average position. As opposed to the case of CM 10 in the Northern Hemisphere, this is not related to a permanent feature of the oceanic circulation. In the Southern Hemisphere for all CMs the ocean transport has two distinct peaks, one located in subtropical and the other one in high-latitude regions. In the case of CMs 1, 4, 6, and 10, the high-latitude peak is typically about as strong as the subtropical one, so that the distribution of location of the yearly maxima of transport is basically bimodal.

[101] When looking at the SRESA1B scenario, we find that all models foresee an increase, ranging from 2% to 12%, in the atmospheric enthalpy transport in both hemispheres. A slight poleward shift is found for the peak of the atmospheric transport in both hemispheres, in broad agreement with what was found by *Yin* [2005]. We have to remark that recent analyses attribute the poleward shift in the Southern Hemisphere to spurious representation of the changes in the cloud cover in altered climate conditions [*Trenberth and Fasullo*, 2010a]. Following *Held and Soden* [2006], the increase in the intensity of the atmospheric

transport may be interpreted as the result of a strong cancelation between the large increase in the poleward latent heat transport, due to the strong enhancement of the hydrological cycle, and the reduction of the sensible heat poleward transport, due to the decrease of the baroclinicity of the system. Recently, *O'Gorman and Schneider* [2008] have shown rather convincingly using a simplified yet Earth-like CM that this compensation mechanism is in place in a rather wide range of climate scenarios.

[102] When considering the ocean's response to CO_2 increase, we find that all CMs foresee a substantial decrease in the intensity of the ocean transport in the Northern Hemisphere, while disagreement exists in the Southern Hemisphere. Typically, a relatively small equatorward shift in the positions of the peaks is found in both hemispheres. These changes partially moderate the observed increase in the atmospheric transport, so that the variations in total meridional transport follow closely but not exactly those of the atmospheric transport: the peak is not shifted systematically in either hemisphere (again, in agreement with *Stone*'s [1978b] argument), while the intensity of the transport is typically increased for most CMs up to 10% in both hemispheres.

[103] The contrasting response to CO_2 concentration increase in the atmospheric and oceanic transports suggests that the Bjerknes compensating mechanism [*Bjerknes*, 1964] is in place on climatological time scales. The yearly time series of the maxima of the atmospheric and oceanic transports have been used also to test (in a very unsophisticated way) whether the Bjerknes mechanism is also active on a shorter time scale. The answer is partially positive, as in both the Northern and the Southern Hemispheres several CMs feature a statistically significant negative correlation between the time series, and other CMs feature statistically nonsignificant correlations, while no cases of significant positive correlations are detected. The mechanism seems to become stronger in warmer climate conditions, possibly as a result of stronger atmosphere-ocean coupling due to more intense latent heat fluxes.

[104] We wish to underline that estimating changes in the net TOA energy balance under altered climate conditions in areas different from zonal bands can provide additional insights on the large-scale climate response. *Fasullo* [2010] showed that in response to increased CO_2 concentration CMs typically foresee an increase of enthalpy transports from ocean to land areas. In fact, as a result of differences in the responses of convection, cloud cover, and cloud vertical structure, the net TOA energy balance decreases over land and increases over ocean. Given the positions of the continents, these results also imply that zonal enthalpy transports will be affected by CO_2 forcing. This is definitely a matter worth exploring in greater detail.

6. CONCLUSIONS

[105] These findings suggest that in spite of the great successes of climate modeling, serious efforts seem to be needed in terms of basic science for substantially improving CMs' performances. This is of great relevance when devising strategies for the future direction to be taken in the development of numerical simulations and is presently of great interest in the context of the preparation of the Fifth Assessment Report of the IPCC. While Earth system science requires models of increasing degrees of complexity that are able to correctly simulate the chemical and biological cycles of our planet and their changes in a changing climate, we cannot expect to improve our understanding of and ability to describe the CS just by indefinitely adding and coupling new modules. Nor can the advocated "quantum leap" in climate simulations be obtained just by improving the computational capabilities [*Shukla et al.*, 2009]. In particular, the definition of strategies for improving the closure of the energy cycle in the fluid components of the CS [*Becker*, 2003] seems to be a crucial step, as important as taking care to consistently represent phase transitions and heat fluxes over land. Some CMs already adopt the strategy of reinjecting into the system the kinetic energy lost to dissipation as a uniform heating term. While this helps in reducing the energy imbalance, it creates regional temperature biases since climate regions featuring almost inviscid, horizontal dynamics are overheated (e.g., the stratosphere), and it defines a spurious source of entropy production as heat is moved down the gradient of the temperature field [*Johnson*, 2000; *Lucarini*, 2009a].

[106] It is apparent that further work is needed to understand why CMs feature in some cases serious biases on the integrated net global energy balances and quantitatively disagree quite substantially, while agreement on qualitative properties is rather satisfactory, on the representation of a fundamental property such as the meridional enthalpy transport. A recent paper suggests that differences in the simulated cloud distribution [see, e.g., *Probst et al.*, 2010] should be considered to be mainly responsible for such discrepancies, whereas surface albedo differences seem to play a minor role (A. Donohoe and D. S. Battisti, Atmospheric and surface contributions to planetary albedo and their relationship to the total meridional energy transport, submitted to *Journal of Climate*, 2010). While in the atmosphere the agreement in the meridional atmospheric transport is reasonable, in the ocean rather different pictures emerge from the various CMs, especially in the Southern Hemisphere. In terms of response to CO_2 increases, whereas we have relatively good agreement in the CMs' responses for the atmospheric transport, a detailed reexamination is required for the ocean response.

[107] The consideration of multimodel ensemble means has often been used as a way to partially circumvent the problem of dealing with CMs' discrepancies [see, e.g., *Held and Soden*, 2006; *Trenberth and Fasullo*, 2009]. The rationale for this choice is that it is often found that such means provide enhanced skill with respect to randomly chosen specific CMs [*Gleckler et al.*, 2008], even if this is far from always being the case [*Lucarini et al.*, 2008]. Although various statistical techniques have been proposed in place of the usual arithmetic average [*Min and Hense*, 2006, 2007; *Tebaldi and Knutti*, 2007] with encouraging empirical results, it must be emphasized that there is no

rigorous statistical ground for combining data from different CMs: outputs of different CMs are *not* samples of the same probability space, and *no* large number law of any sort applies [*Lucarini*, 2008, 2009b]. Thus, a detailed understanding of CMs' uncertainties and discrepancies is of the greatest urgency.

[108] In general, advances in numerical schemes as well as in the representation of physical processes are needed for providing a well-defined and self-consistent representation of climate as a nonequilibrium thermodynamical system when long time scales and large spatial scales are considered. Furthermore, additional work is needed in the definition of suitable metrics for the investigation of the global thermodynamical properties of the CS and in testing the performances of state-of-the-art and future generations of CMs. Along these lines, and stimulated by recent extensive scholarly reviews [*Ozawa et al.*, 2003; *Wu and Liu*, 2010], the authors are preparing a companion publication dealing with the analysis of the entropy production [*Ozawa et al.*, 2003; *Lucarini*, 2009a] of PCMDI CMIP3 CMs. Recently, V. Lucarini et al. (Bounds on the thermodynamical properties of the fluid envelope of a planet based upon its radiative budget at the top of the atmosphere: Theory and results for Earth, Mars, Titan, and Venus, submitted to *Journal of the Atmospheric Sciences*, 2010) have shown that it is possible to estimate the total entropy production of the CS just by analyzing the TOA and surface longwave and shortwave radiative fluxes and to separate the contributions due to vertical, small-scale processes from those due to horizontal, large-scale processes.

[109] We suggest that the PCMDI CMIP5 initiative, which will specifically take care of providing the tools necessary for auditing the present and future generations of climate and Earth system models, should take greater care to provide data referring to simulations by CMs under steady state with various choices of basic parameters, such as the solar constant (e.g., ±2% of the present one) and the CO_2 (e.g., 275, 550, and 1000 ppm), and should make it possible for research groups to access the data necessary for the analysis of the energy and entropy budgets of the planet. While these simulations and data sets might seem unnecessary and not of direct impact for the assessment of the actual and projected climate change, they would allow for a much more detailed understanding of the performance of CMs. Of course, it is crucial for matters of self-consistency that the energy bias of a CM is as small as possible in all steady state scenarios. It is manifest that climate-dependent energy biases may contribute to increasing the uncertainty in the climate sensitivity, and we may conjecture that this may play a role in the relatively large discrepancies among state-of-the-art CMs on the definition of this crucial quantity (still spanning between 2°C and 4.5°C) and, correspondingly, of the change in the globally averaged surface temperature resulting from historical and projected CO_2 concentration increases [*Solomon et al.*, 2007].

[110] We conclude by noting that most of the results presented here could also be applied to studying the climates of celestial bodies such as planets and satellites. This is a rather promising and exciting perspective because apart from the everlasting interest in the solar planets and satellites, we live in the dawn of the era of extrasolar planet and satellite science. Therefore, what we have reviewed here as well as the ongoing studies on the entropy production and efficiency of the Earth system may be of help for studying the thermodynamics of the atmospheres of celestial bodies. Thus, it is encouraging to observe that various models belonging to the PLASIM family have already been adapted to study the atmospheres of Titan [*Grieger et al.*, 2004] and Mars [*Stenzel et al.*, 2007] and that intercomparison projects on the modeling of the Venusian atmosphere (see http://www.issibern.ch/workshops/venusclimate/) and Martian atmosphere (see http://www.atm.ox.ac.uk/user/newmanc/workshop/intercomp.html) are ongoing.

REFERENCES

Allan, R. P., M. A. Ringer, J. A. Pamment, and A. Slingo (2004), Simulation of the Earth's radiation budget by the European Centre for Medium-Range Weather Forecasts 40-year reanalysis (ERA40), *J. Geophys. Res.*, *109*, D18107, doi:10.1029/2004JD004816.

Ambaum, M. (2010), *Thermal Physics of the Atmosphere*, John Wiley, New York.

Becker, E. (2003), Frictional heating in global climate models, *Mon. Weather Rev.*, *131*, 508–520.

Bjerknes, J. (1964), Atlantic air-sea interaction, in *Advances in Geophysics*, edited by H. E. Landsberg and J. van Mieghem, pp. 1–82, Academic, New York.

Carissimo, B., A. Oort, and T. Haar (1985), Estimating the meridional energy transports in the atmosphere and ocean, *J. Phys. Oceanogr.*, *15*, 82–91.

de Groot, J., and A. Mazur (1962), *Nonequilibrium Thermodynamics*, North-Holland, Amsterdam.

Dell'Aquila, A., V. Lucarini, P. Ruti, and S. Calmanti (2005), Hayashi spectra of the Northern Hemisphere mid-latitude atmospheric variability in the NCEP-NCAR and ECMWF reanalyses, *Clim. Dyn.*, *25*, 639–652.

Dell'Aquila, A., P. M. Ruti, S. Calmanti, and V. Lucarini (2007), Southern Hemisphere midlatitude atmospheric variability of the NCEP-NCAR and ECMWF reanalyses, *J. Geophys. Res.*, *112*, D08106, doi:10.1029/2006JD007376.

Enderton, D., and J. Marshall (2009), Explorations of the atmosphere-ocean-ice climates on an aquaplanet and their meridional energy transports, *J. Clim.*, *22*, 1593–1611.

Fasullo, J. T. (2010), Robust land-ocean contrasts in energy and water cycle feedbacks, *J. Clim.*, 23, 4677–4693, doi:10.1175/2010JCLI3451.1.

Fermi, E. (1956), *Thermodynamics*, Dover, New York.

Fraedrich, K., H. Jansen, E. Kirk, U. Luksch, and F. Lunkeit (2005), The planet simulator: Towards a user friendly model, *Meteorol. Z.*, 14, 299-304.

Frierson, D., I. Held, and P. Zurita-Gotor (2007), A gray-radiation aquaplanet moist GCM. Part II: Energy transports in altered climates, *J. Atmos. Sci.*, 64, 1680–1693.

Gallavotti, G. (2006), Nonequilibrium statistical mechanics (stationary): Overview, in *Encyclopedia of Mathematical Physics*, edited by J.-P. Françoise, G. L. Naber, and T. S. Tsun, pp. 530–539, Elsevier, Amsterdam.

Gleckler, P. J., K. E. Taylor, and C. Doutriaux (2008), Performance metrics for climate models, *J. Geophys. Res.*, 113, D06104, doi:10.1029/2007JD008972.

Goody, R. (2000), Sources and sinks of climate entropy, *Q. J. R. Meteorol. Soc.*, 126, 1953–1970.

Grieger, B., J. Segschenider, H. Keller, A. Rodin, F. Lunkeit, E. Kirk, and K. Fraedrich (2004), Simulating Titan's tropospheric circulation with the Portable University Model of the Atmosphere, *Adv. Space Res.*, 34, 1650–1654.

Held, I. (2005), The gap between simulation and understanding in climate modeling, *Bull. Am. Meteorol. Soc.*, 86, 1609–1614.

Held, I., and B. Soden (2006), Robust responses of the hydrological cycle over to global warming, *J. Clim.*, 19, 5686–5699.

Johnson, D. (1997), General coldness of climate models and the second law: Implications for modeling the Earth system, *J. Clim.*, 10, 2826–2846.

Johnson, D. (2000), Entropy, the Lorenz energy cycle and climate, in *General Circulation Model Development: Past, Present and Future*, edited by D. Randall, pp. 659–720, Academic, New York.

Kiehl, J., and K. Trenberth (1997), Earth's annual global mean energy budget, *Bull. Am. Meteorol. Soc.*, 78, 197–208.

Kleidon, A., and R. Lorenz (2005), *Non-equilibrium Thermodynamics and the Production of Entropy: Life, Earth and Beyond*, Springer, New York.

Kuhlbrodt, T., A. Griesel, M. Montoya, A. Levermann, M. Hofmann, and S. Rahmstorf (2007), On the driving processes of the Atlantic meridional overturning circulation, *Rev. Geophys.*, 45, RG2001, doi:10.1029/2004RG000166.

Kundu, P., and I. Cohen (2008), *Fluid Mechanics*, Academic, San Diego, Calif.

Lenton, T., H. Held, E. Kriegler, J. Hall, W. Lucht, S. Rahmstorf, and H. Schellnhuber (2008), Tipping elements in the Earth's climate system, *Proc. Natl. Acad. Sci. U. S. A.*, 105, 1786–1793.

Lorenz, E. (1955), Available potential energy and the maintenance of the general circulation, *Tellus*, 7, 157–167.

Lorenz, E. (1967), *The Nature and Theory of the General Circulation of the Atmosphere*, World Meteorol. Organ., Geneva, Switzerland.

Lucarini, V. (2002), Towards a definition of climate science, *Int. J. Environ. Sci.*, 18, 413–422.

Lucarini, V. (2008), Validation of climate models, in *Encyclopedia of Global Warming and Climate Change*, edited by G. Philander, pp. 1053–1057, SAGE, Thousand Oaks, Calif.

Lucarini, V. (2009a), Thermodynamic efficiency and entropy production in the climate system, *Phys. Rev. E*, 80, 021118.

Lucarini, V. (2009b), Evidence of dispersion relations for the nonlinear response of the Lorenz 63 system, *J. Stat. Phys.*, 134, 381–400.

Lucarini, V., and K. Fraedrich (2009), Symmetry-break, mixing, instability, and low frequency variability in a minimal Lorenz-like system, *Phys. Rev. E*, 80, 026313.

Lucarini, V., and G. L. Russell (2002), Comparison of mean climate trends in the Northern Hemisphere between National Centers for Environmental Prediction and two atmosphere-ocean model forced runs, *J. Geophys. Res.*, 107(D15), 4269, doi:10.1029/2001JD001247.

Lucarini, V., T. Nanni, and A. Speranza (2006), Statistical properties of the seasonal cycle in the mediterranean area, *Nuovo Cimento Soc. Ital. Fis. C*, 29, 21–31.

Lucarini, V., S. Calmanti, A. Dell'Aquila, P. Ruti, and A. Speranza (2007), Intercomparison of the Northern Hemisphere winter mid-latitude atmospheric variability of the IPCC models, *Clim. Dyn.*, 28, 829–848.

Lucarini, V., R. Danihlik, I. Kriegerova, and A. Speranza (2008), Hydrological cycle in the Danube basin in present-day and XXII century simulations by IPCCAR4 global climate models, *J. Geophys. Res.*, 113, D09107, doi:10.1029/2007JD009167.

Lucarini, V., K. Fraedrich, and F. Lunkeit (2010a), Thermodynamic analysis of snowball Earth hysteresis experiment: Efficiency, entropy production, and irreversibility, *Q. J. R. Meteorol. Soc.*, 136, 2–11.

Lucarini, V., K. Fraedrich, and F. Lunkeit (2010b), Thermodynamics of climate change: Generalized sensitivities, *Atmos. Chem. Phys. Discuss.*, 10, 3699–3715.

Min, S.-K., and A. Hense (2006), A Bayesian assessment of climate change using multimodel ensembles. Part I: Global mean surface temperature, *J. Clim.*, 19, 3237–3256.

Min, S.-K., and A. Hense (2007), Hierarchical evaluation of IPCC AR4 coupled climate models, *Clim. Dyn.*, 29, 853–868.

Nakamura, M., P. H. Stone, and J. Marotzke (1994), Destabilization of the thermohaline circulation by atmospheric eddy transports, *J. Clim.*, 12, 1870–1882.

O'Gorman, P., and T. Schneider (2008), The hydrological cycle over a wide range of climate simulated with an idealized GCM, *J. Clim.*, 21, 3815–3832.

Ozawa, H., A. Ohmura, R. D. Lorenz, and T. Pujol (2003), The second law of thermodynamics and the global climate system: A review of the maximum entropy production principle, *Rev. Geophys.*, 41(4), 1018, doi:10.1029/2002RG000113.

Peixoto, J., and A. Oort (1992), *Physics of Climate*, Springer, New York.

Philander, S., D. Gu, G. Lambert, T. Li, D. Halpern, N. Lau, and R. Pacanowski (1996), Why the ITCZ is mostly north of the equator, *J. Clim.*, 9, 2958–2972.

Prigogine, I. (1961), *Thermodynamics of Irreversible Processes*, Interscience, New York.

Probst, P., R. Rizzi, E. Tosi, V. Lucarini, and T. Maestri (2010), Total cloud cover from satellite observations and climate models, *Atmos. Chem. Phys. Discuss.*, 10, 21,023–21,046.

Saltzmann, B. (2002), *Dynamical Paleoclimatology*, Academic, New York.

Schneider, T. (2006), The general circulation of the atmosphere, *Annu. Rev. Earth Planet. Sci.*, 34, 655–688.

Shaffrey, L., and R. Sutton (2006), Bjerknes compensation and the decadal variability of the energy transports in a coupled climate model, *J. Clim.*, 19, 1167–1181.

Shukla, J., R. Hagedorn, M. Miller, T. N. Palmer, B. Hoskins, J. Kinter, J. Marotzke, and J. Slingo (2009), Revolution in climate prediction is both necessary and possible: A declaration at the world modelling summit for climate prediction, *Bull. Am. Meteorol. Soc.*, 90, 175–178.

Solomon, S., D. Qin, M. Manning, Z. Chen, M. Marquis, K. B. Averyt, M. Tignor, and H. L. Miller (Eds.) (2007), *Climate Change 2007: The Physical Science Basis. Contribution of Working Group I to the Fourth Assessment Report of the Intergovernmental Panel on Climate Change*, 996 pp., Cambridge Univ. Press, Cambridge, U. K.

Stenzel, O. J., B. Grieger, H. U. Keller, K. Fraedrich, E. Kirk, and F. Lunkeit (2007), Coupling Planet Simulator Mars, a general circulation model of the Martian atmosphere, to the ice sheet model SICOPOLIS, *Planet. Space Sci.*, 355, 2087–2096.

Stone, P. (1978a), Baroclinic adjustment, *J. Atmos. Sci.*, 35, 561–571.

Stone, P. (1978b), Constraints on dynamical transports of energy on a spherical planet, *Dyn. Atmos. Oceans*, *2*, 123–139.

Tebaldi, C., and R. Knutti (2007), The use of the multi-model ensemble in probabilistic climate projections, *Philos. Trans. R. Soc. A*, *365*, 2053–2076.

Trenberth, K. (1991), Storm tracks in the Southern Hemisphere, *J. Atmos. Sci.*, *48*, 2159–2178.

Trenberth, K., and J. Caron (2001), Estimates of meridional atmosphere and ocean heat transports, *J. Clim.*, *14*, 3433–3443.

Trenberth, K. E., and J. T. Fasullo (2009), Global warming due to increasing absorbed solar radiation, *Geophys. Res. Lett.*, *36*, L07706, doi:10.1029/2009GL037527.

Trenberth, K., and J. Fasullo (2010a), Simulation of present-day and twenty-first-century energy budgets of the southern oceans, *J. Clim.*, *23*, 440–454.

Trenberth, K., and J. Fasullo (2010b), Tracking Earth's energy, *Science*, *328*, 316–317.

Trenberth, K., and D. Stepaniak (2003), Seamless poleward atmospheric energy transports and implications for the Hadley circulation, *J. Clim.*, *16*, 3706–3722.

Trenberth, K., J. Fasullo, and J. Kiehl (2009), Earth's global energy budget, *Bull. Am. Meteorol. Soc.*, *90*, 311–323.

Vallis, G., and R. Farneti (2009), Meridional energy transport in the coupled atmosphere-ocean system: Scaling and numerical experiments, *Q. J. R. Meteorol. Soc.*, *135*, 1643–1660.

van der Swaluw, E., S. S. Drijfhout, and W. Hazeleger (2007), Bjerknes compensation at high northern latitudes: The ocean forcing the atmosphere, *J. Clim.*, *20*, 6023–6032.

Wild, M. (2008), Shortwave and longwave surface radiation budgets in GCMs: A review based on the IPCC-AR4/CMIP3 models, *Tellus, Ser. A*, *60*, 932–945.

Wild, M., C. N. Long, and A. Ohmura (2006), Evaluation of clear-sky solar fluxes in GCMs participating in AMIP and IPCC-AR4 from a surface perspective, *J. Geophys. Res.*, *111*, D01104, doi:10.1029/2005JD006118.

Wilks, D. (2005), Resampling hypothesis tests for autocorrelated field, *J. Clim.*, *10*, 65–82.

Wu, W., and Y. Liu (2010), Radiation entropy flux and entropy production of the Earth system, *Rev. Geophys.*, *48*, RG2003, doi:10.1029/2008RG000275.

Yang, S.-K., Y.-T. Hou, A.-J. Miller, and K. Campana (1999), Evaluation of the Earth radiation budget in NCEP-NCAR reanalysis with ERBE, *J. Clim.*, *12*, 477–493.

Yin, J. H. (2005), A consistent poleward shift of the storm tracks in simulations of 21st century climate, *Geophys. Res. Lett.*, *32*, L18701, doi:10.1029/2005GL023684.

V. Lucarini, Department of Meteorology, University of Reading, Earley Gate, PO Box 243, Reading RG6 6BB, UK. (v.lucarini@reading.ac.uk)

F. Ragone, Meteorologisches Institut, KlimaCampus, University of Hamburg, Grindelberg 5, Hamburg D-20144, Germany.